DUANE ARNOLD ENERGY CENTER

RECIRCULATION INLET
SAFE END REPAIR PROGRAM
SUPPLEMENT

February 22, 1979

INDEX

JLR:cas/61B12

I. INTRODUCTION

The purpose of this Iowa Electric Light and Power Company (IE) Report is to supplement the information presented in the Duane Arnold Energy Center Recirculation Inlet Safe End Repair Program Report, dated December 8, 1978.

This Supplemental Report primarily addresses two topics which were raised subsequent to submittal of the December 8, 1978 Repair Report: (1) the acceptability of recirculation inlet safe end welds #2 and #6 (Figure I.A-1); and (2) the procedure for the recovery of one lead plug, including ten lead bricks and several component parts, left in nozzle N2B after completion of the safe end repair welding.

In accepting welds #2 and #6, IE has obtained the radiographic interpretation of six people certified or qualified to ASNT Level III requirements. This Supplemental Report includes a detailed explanation of the criteria and analysis employed by IE to determine weld acceptability in accordance with ASME Boiler and Pressure Vessel Code Section III subsections NB-4424 and NB-5320. All six individuals who examined the radiographs in question determined that the welds meet Code.

In addition to the weld acceptance process utilized by IE, the Supplemental Report includes analyses of welds #2 and #6 with regard to oxide film effects, stress and fatigue, and ultrasonic inspectability.

Sections III and IV of this Supplemental Report discuss the disposition of the lead shield plugs and component parts, including IE's lead brick recovery procedure, an analysis of the impact of lead smears on the stress corrosion cracking resistance of Alloy 600 , and IE's proposed procedure for lead smear removal, using the reactor water cleanup system.

Finally, this Supplemental Report amplifies the information and analyses presented in the December 8, 1978 Repair Report on the following topics: Alloy 600 crack propagation rate analysis; maximum flaw acceptability analysis; leak before break analysis; IE's proposed inservice inspection program for the repaired recirculation inlet safe ends; and IE's leak detection hardware and history.

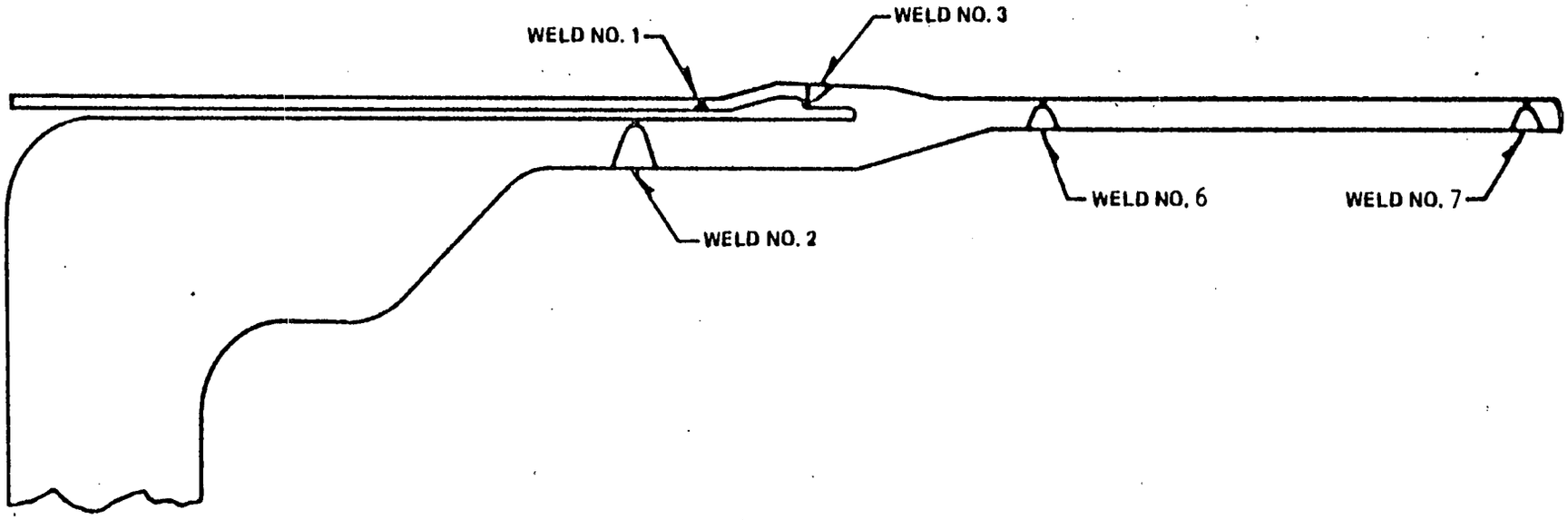

FIGURE I.A-1

II.A ACCEPTANCE OF WELDS

1. Weld Acceptance Process

This section describes the criteria by which Iowa Electric determined the weld acceptability and the analysis which establishes the level of acceptability.

A. Code Requirement

The ASME Boiler and Pressure Vessel Code Section III subsection NB-4424 and NB-5320 provide criteria for assisting in the determination of acceptability of welds. Subsection NB-4424 deals with surfaces of welds and gives a basis for assuring absence of coarse ripples, grooves, overlaps, and abrupt ridges and valleys. Subsection 5320 deals with radiographic acceptance standards for welds. This subsection identifies unacceptable discontinuites which may indicate incomplete fusion or incomplete penetration and other unacceptable elongated indications.

These subsections provide a basis for interpreting weld radiographs to determine weld acceptability. The intent of the code is to provide a process for evaluating the technical merits of each weld. The code is used when interpreting radiographs to locate potential unacceptable weld areas. Each questionable weld area is then evaluated to determine its adequacy.

The ASME Code requires that the repair welds be acceptable to NDE personnel qualified in accordance with NB-5500. The welds were examined and accepted by six people certified or qualified to ASNT Level III requirements.

B. Radiograph Review

Following each root weld, a radiograph was taken and examined to assure full fusion and penetration. The root weld radiograph was also used to determine acceptability of the root surface from concavity and oxidation.

The root weld radiograph was judged acceptable before continuing with the final weld passes. During the remaining weld pass, where the potential for unacceptable conditions existed, radiographs were taken to determine intermediate status of the weld. Final weld acceptance was determined based on examination of the final weld radiograph.

C. Interpretation of Radiographs

Each radiograph was scanned for potential irregularities and checked for acceptable film density. Each irregularity was examined for potential unacceptable concavity and thickness through the root section of the weld. The film density was

compared through the root section and the base metal. A micro scan was used to identify potential abrupt changes and establish a profile of the root surface. A range of root geometries was evaluated for design load conditions and compared to code stresses and the General Electric Stress Rule Index. Weld thickness was also compared to results from ultrasonic examination to confirm thicknesses taken from radiograph examinations. When the potential for oxidation at irregular surfaces existed other indications of penetration of oxygen into the effected area of the weld were found to be absent.

Where irregularities would possibly indicate presence of a crevice condition at the weld inner surface, capability for coolant flushing has been assessed and found to be adequate. Therefore, concern for possible crevice conditions does not exist.

A micro-scanning densitometer device at Newport News Industrial was utilized to provide additional information to substantiate earlier evaluations. Documentation for its use is contained in an instruction manual for the device. This device is basically an optical comparitor which was utilized to compare radiographic film density changes.

Radiographic density changes are observed as light intensity changes which were then translated into graphic form. The principle of operation is based on a double-beam light system

in which two beams from a single light source are switched alternately to a single photo-electric receiver. If the two beams are of a different intensity, a signal is produced by the photo-multiplier, which after multiplication causes a servo motor to move an optical attenuator so as to reduce the intensity difference to zero. In this way a continuously null balancing system is obtained. No unique calibration records are required because the device is calibrated by the operator during each usage by correlating the graphic trace to a known thickness.

The direct linkage between the specimen and the record table assures complete synchronization, irrespective of the ratio by which the record is expanded with respect to the specimen. The device was maintained and operated by Newport News personnel who utilize this same device for U.S. Navy work. Repeatability was verified on Duane Arnold Energy Center work by subsequent review activities.

JLR:cas/61B9

2. Detailed Evaluation of Welds

All repair welds have been analyzed based on evaluation of radiographs. The NRC has raised questions on interpretation of radiographs for nine welds. The following discusses the observations and conclusions reached for these welds. A detailed discussion of each weld is contained in Table II.A.

3. Final Conclusion

As stated in Section II all repair welds have been accepted based on radiographs of each root and final weld. Although the NRC has raised some questions about interpretation of some radiographs, each question has been evaluated and the conclusion reached by Iowa Electric is that the welds are acceptable based on the technical merits of each weld. In some cases where the possibility of oxidation exists based on radiographic interpretation of the surface of the root weld, it is concluded that the surface oxidation has not penetrated into the effective weld area. It has been concluded that potential irregularities will not create potential crevice conditions because adequate circulating coolant flushing exists. In those cases where concavity of the inner surface potentially exists, it is concluded that the small amount of concavity does not limit the weld to withstand the intended design loads. The resulting stresses and stress rule index is within acceptable limits. In those cases where density changes exist it has been judged that the density changes are not sufficiently abrupt to indicate lack of weld fusion or lack of weld penetration.

TABLE II.A-1

Weld Radiograph Examinations

Nozzle/Weld	Film	Location	Observation	Evaluation
A/2 Final Root	0-14	4	Tungsten inclusion	Acceptable Within the limits of NB-5320
	14-28	18-25	Intermittent spots of protruding metal on ID	There is no evidence of elongated indications at the edge of the protruding metal which was caused by irregularity in consumption of the insert. Acceptable
	28-0	31½	Tungsten inclusion	Within the limits of NB-5320. Acceptable
A/2 Final Weld	0-14	3-11	Minor porosity and a tungsten inclusion	Within the limits of NB-5320. Acceptable
	14-28	14-22	Minor porosity	Within the limits of NB-5320. Acceptable
		18-25	Intermittent spots of protruding metal on weld ID	
	27-0	27-40	Minor porosity and tungsten inclusion	Within the limits of NB-5320. Acceptable

Weld Radiograph Examinations

Nozzle/Weld	Film	Location	Observation	Evaluation
B/2 Root	0-8	0-2½	Convexity in root with light oxidation	No evidence of lack of fusion or elongated indications at edge of convexity. Acceptable.
	8-16	11 and 16	Irregularity in breakdown insert	Acceptable.
	16-0	19 3/4	High and low spots adjacent in root	No evidence of non-fusion or elongated indications at edges of root. Acceptable.
		20-22½	High one side of root and low on other	
		22½-0	Convexity with light oxidation	
B/2 Final Weld	0-14	0-5	Convexity with light oxidation	No evidence of lack of fusion or elongated indications at edge of convexity. Acceptable
		0-14	Minor slag, porosity and tungsten	
	14-28	16-19	Porosity	Within the limits of NB-5320. Acceptable
	28-0	41-0	Convexity with light oxidation	No evidence of lack of fusion. No elongated indications at edge of convexity. Acceptable.
				Micro-scan densitometer scans were made at 2 3/4 and at 6. There were no elongated indications at the edge of the convexity at 2 3/4 and there was no abrupt changes in density at the root at 6.

Weld Radiograph Examinations

Nozzle/Weld	Film	Location	Observation	Evaluation
B/6 Root	0-8		No Apparent Defects	Acceptable
	8-16		No Apparent Defects	Acceptable
	16-24	15½	Burn-through which was later repaired and reshot on Film R2	Rejected on this film but was repaired and reshot on the film R2 dated 12/6/78 shown below
	24-0		No Apparent Defects	Acceptable
	12-28 dated 12/6/78 and marked R2	14-17	Wide concavity with weld rod that was push thru is fused to root ID. Rod was subsequently ground out and grind-out was rewelded.	The concavity is approximately ¼" wide. There is no evidence of non-fusion or abrupt changes in density. Acceptable to complete weld.
B/6 Final Weld	0-8		No Apparent Defects	Acceptable
	8-16	13-15	Concavity that is about 1/8" wide and approximately 2" long. Densitometer checks proved the thickness of the weld through the concave area was thicker than the base metal.	There is no evidence of non-fusion or abrupt changes in density. Acceptable. Subsequent shots were made with grooved block for evaluation of concavity with the micro-scan densitometer.
	16-24		No Apparent Defects	Acceptable

Weld Radiograph Examinations

Nozzle/Weld	Film	Location	Observation	Evaluation
B/6 Final Weld (Continued)	24-0		NAD	Acceptable
B/6 Final Weld Single film made with grooved shim block	12-18	12½ 14½-16½	Density Change Indicating Rounded area of concavity Concavity	This film was made with a grooved shim block placed adjacent to the weld which provided means to profile the concavity with the microscan densitometer. Scans were made at locations 12 3/4", 15, 15 3/8 and 15 3/4. The maximum net depth of the concavity was .017", and the scans showed no abrupt changes in density. Accepted.

JLR:cas/61K1

Weld Radiograph Examinations

Nozzle/Weld	Film	Location	Observation	Evaluation
C/2 Root Plus 1 Filler Pass	0-14		No apparent defects	Acceptable
	14-28	14-25	Shallow concavity	There is no evidence of non-fusion or elongated indications. Acceptable.
		19-23	Stringer type convexity with possible light oxidation	
	28-0		No apparent defects	Acceptable
C/2 Final Weld	0-13	0-10	Small scattered porosity	Within the limits of NB-5320. Acceptable.
	13-28	13½-20½	Shallow concavity	Micro-scan densitometer readings were made at 17¼ and 19 3/4 which showed no abrupt changes in density. Density readings confirm that all root areas are thicker than base metal. In addition, ultrasonic measurements taken at 16, 21, and 24½ confirm the thickness of the weld root and base metal. There is no evidence of non-fusion or elongated indications in the root. The weld is acceptable.
		20½-21½	Moderate convexity with shallow centerline concavity	
		21½-23½	Stringer type convexity	
		24-25	Concavity	
	28-0	29½-42	Small tungsten inclusions	Within the limits of NB-5320. Acceptable.

JLR:cas/61K2

Weld Radiograph Examinations

Nozzle/Weld	Film	Location	Observation	Evaluation
D/2 Final Root	0-14	2-4, 7	Convexity and Oxidation	Oxidation is on material protruding inside pipe I.D. and we see no elongated indication at the edge of protruding metal. Acceptable. No elongated indications. Acceptable.
	14-28	17-23 21-25	Concavity intermittent stringer type convexity and oxidation	No abrupt change in density in concave area. Oxidation is on material protruding inside pipe I.D. Acceptable. No elongated indications. Acceptable.
	28-40	37-39	Stringer type convexity and oxidation	Same comments as above. Acceptable.
D/2 Final Weld	0-14	3-5, 8 0-10	Convexity and oxidation scattered small porosity indications	Same as above
	14-28	17-24 22-25	Concavity stringer type convexity and oxidation	Same as above
	28-0	37-39	Stringer type convexity and light oxidation	Same as above

JLR:cas/61K3

Weld Radiograph Examinations

Nozzle/Weld	Film	Location	Observation	Evaluation
D/2 Final Weld (Continued)				Microscans taken at 3½, 18, 19, 23 7/8 (concave and convex sections). Convex sections show high ridge at center but no sharp discontinuity at edge of root. Concave sections show density changes. Visual examination with magnification was made in the zones of concavity which exhibited density changes. No indications of rejected defects per NB 4424 and NB 5320 were noted. Density readings confirm that all sections through the root are thicker than adjoining base metal. Confirmed with ultrasonic measurement. Conclusion is that the weld meets the requirements of NB 4424 and NB 5320 and is acceptable.

JLR:cas/61K4

Weld Radiograph Examinations

Nozzle/Weld	Film	Location	Observation	Evaluation
E/2 Root Hot Pass	0-14	10-14	Moderate concavity	There is no evidence of non-fusion or elongated indications at the edges of the root. Oxidation is only on the surface of the metal protruding at the root and is not in the effective cross section of the weld. Acceptable.
		13½-14	Convexity with light oxidation	
	14-28	14-15½	Convexity with light oxidation	Same as above. Acceptable.
		15½-17½	Moderate concavity	
		17½-26½	Crease type convexity with light oxidation	
		27-28	Moderate concavity	
	28-0	28-32	Moderate concavity	Same as above. Acceptable.
E/2 Final Weld	0-14	10-14	Moderate concavity	There is no evidence of non-fusion or elongated indication at the edges of the root. Density reading confirmed that the weld was thicker through the root section than the base metal. Also, UT readings at 13, 17 and 22 confirmed the thickness comparison. Microscans were made at loctions 10, 12, 17½, 20, 26 and 31. There was no evidence of abrupt density changes at the edge of the root at the concave reas. Also, there was no evidence of elongated indications at the edges of the convex areas. The weld is acceptable.
		14	Convexity with light oxidation	
	14-28	14-16	Convexity with light oxidation	
		17½-26½	Crease type convexity with light oxidation	
		27-28	Moderate concavity	
	28-0	28-32	Moderate concavity	

JLR:cas/61K5

Weld Radiograph Examinations

Nozzle/Weld	Film	Location	Observation	Evaluation
E/6 Final Root	0-8		No apparent defects	Well contoured root.
	8-16	15-16	Minor Concavity	
	16-26	17-19 19 22-26	Wide Concavity Stringer Convexity Shallow concavity through three short zones of melt-through	No abrupt changes in density in concave and convex areas. Residual melt-through with smooth interface and no elongated indications.
	26-0	26-29	Shallow Concavity through two short melt-through zones	
		31-34	Melt-through with slight indications of oxidation	Oxidation is on material protruding inside pipe I.D. No elongated indications.
E/6 Final Weld	0-8		No apparent defects	
	8-16	13-16	Concavity	
	16-26	16-18	Light Concavity	Same comments as above
		19-26	Light Concavity through three short melt-through zones	Density readings confirm that all sections through the root are thicker than adjoining base metal.
		19	Short stringer convexity	

JLR:cas/61K6

Weld Radiograph Examinations

Nozzle/Weld	Film	Location	Observation	Evaluation
E/6 Final Weld (Continued)	26-0	26-30	Shallow Concavity throught two short melt-through zones	Same comments as above
		31-34	Melt-through with slight indication of oxidation	Ultrasonic scans taken at four locations across width of weld and one location at base metal safe-end extension side at weld at one-fourth inch intervals on circumference at weld from location 13½ to 31. In every case weld metal was thicker than base metal.
E/6 Final Weld (Single film taken with grooved shim block)	14-25	15½-22	Concavity	In areas of concavity (Location 14-25) radiograph taken with grooved shim block to check contour and depth of the root. Using a micro-scan densitometer, the weld was scanned at 15½, 16 3/4, 17½, 18¼, 21¼, and 22. The maximum concavity including the necking of the base material was 0.047 in. compared to original base material depth. The maximum net concavity compared to the base material (not including base material necking) was 0.030 inches maximum. The grooved shim block was effectively used to provide linear calibration of cavity depth measurement. No indication of abruptness was seen at the edges of the root from the microscans. Subsequent stress evaluation concluded that the weld was acceptable.

JLR:cas/61K7

Weld Radiograph Examinations

Nozzle/Weld	Film	Location	Observation	Evaluation
G/2 Root	0-14		No apparent defects	Acceptable
	14-28	18-26	Convex center line crease with surface oxidation	There is no evidence of elongated indication at the edge of the convex area and the surface oxidation is only on the protruding metal. Acceptable.
		27	Moderate concavity approximately 3/4" long	There is no evidence of abrupt change in density at the edge of the concave area.
	28-0		No apparent defects	Acceptable
G/2 Final Weld	0-14	0-2	Minor porosity and slag	Acceptable
	14-28	17, 20, 28	Moderate concavity at these three locations	There is no evidence of non-fusion or elongated indication at the edge of the root. Density readings confirmed that the weld was thicker through the root section than the base metal. Also, UT readings at 17, 19½, 24 and 26 confirmed the thickness comparison. There is no evidence of abrupt density change at the edges of root in the concave areas. Also, there is no evidence of elongated indications at the edge of the convex areas. The weld is acceptable.
		17½-25	Convex centerline crease with surface oxidation	
	28-0	28-40	Minor porosity, slag and one tungsten inclusion	Acceptable

JLR:cas/61K8

Weld Radiograph Examinations

Nozzle/Weld	Film	Location	Observation	Evaluation
H/2 Root and one Filler Pass	1-7	0-2½	Small tungsten inclusions undercut at edge of root	Within limits of NB 5320. Acceptable.
		5¼		Acceptable per the provisions of NB 4424C
	7-14	9-10½	Moderate convexity with possible light oxidation	There is no evidence of elongated indications at edges of convexity. Acceptable.
	14-0	15½-15 3/4	Crease type convexity with possible light oxidation	Same as above.
		20-0	Moderately convex root with intermittent light oxidation	Same as above.
		16-17	Moderate concavity	There is no evidence of non-fusion or abrupt change in density or elongated indication at the edges of the root.
		18	The back scatter letter "B" was inadvertently placed on the source side of the film	
H/2 Final Film	D-14	11½	Same location as 5½ on root film. Has appearances of minor undercut at edge of root.	Evaluated as a minor undercut at the root and is within acceptable limits. No evidence of an elongated indication.
		13-14½	Moderate concavity	Acceptable.

JLR:cas/61K9

Weld Radiograph Examinations

Nozzle/Weld	Film	Location	Observation	Evaluation
H/2 Final Film (Continued)	14½-28	16	Moderate concavity	Acceptable
		17½-19½	Moderate concavity with moderate convexity at one edge	Acceptable
		20	Short convex area	Acceptable
	28-0	28-34	Unevenly consumed insert	No evidence of lack of fusion or elongated indications. Acceptable. Density readings confirmed that the weld was thicker than the base metal and was confirmed by UT at locations 11, 16½ and 28½. Microscans at 11½, 16½, 18, 19, 28 and 28½ confirmed that there were no abrupt changes. The weld is acceptable.

JLR:cas/61K10

II.B THE EFFECTS OF AN OXIDE FILM ON THE IGSCC RESPONSE OF ALLOY 600

Introduction

Recent investigations have indicated that some localized areas of the replacement safe end welds on Duane Arnold Alloy 600 recirculation inlet safe ends may be partly covered with an oxide film or scale resulting from the welding operation. It was considered prudent to determine if the presence of an oxide film on the Alloy 600 weld surface would significantly affect the material's inherent intergranular stress corrosion cracking (IGSCC) resistance. Therefore, this review was undertaken to examine the relevant basic engineering information concerning the oxide film - IGSCC interaction. This review was somewhat hampered by the paucity and fragmentary nature of the available relevant data, especially in the specific case of Alloy 600 with a heavy oxide scale exposed to typical BWR environments. However, sufficient data was found to allow some sound engineering judgments to be made.

Results

Berry et. al.[1] investigated the IGSCC behavior of furnace sensitized Type 304 stainless steel in 288°C (550°F) primary water as a function of various operating parameters such as oxygen and fluoride contents of the

water, stress level, prestrain, heat treatment and surface preparation (tarnish film, surface ground or pickled.) The surface preparation results are of prime consideration for this review.

Constant load tests were performed on tensile bars and pressurized tubes of two heats of Type 304 (0.051 and 0.060 w/o C) sensitized at 621°C (1150°F) for 7 or 24 hours to produce a light and heavy tarnish, respectively. Since non-tarnished sample results indicated that the sensitization produced by 7 and 24 hours at 621°C appeared to be approximately equal in producing susceptibility to IGSCC, it was believed that the effect of the degree of tarnishing would be revealed by this study. The results of this investigation are summarized in Table I and described below.

The experimental results indicated that there was insignificant difference between specimens receiving the two tarnishes. Twenty of the 69 specimens cracked; 13 tarnished specimens, 2 dry abraded specimens and 5 pickled specimens. The overall corresponding percentage cracking was 33% tarnished, 10% abraded and 83% pickled. The results initially seem to indicate that removing the tarnish film by abrading reduces the possibility of IGSCC. However, closer examination of the limited data for the simulated BWR 0.2 ppm oxygen environment with highly stressed (3.Sm) and heavily sensitized specimens reveals that 40% of the tarnished specimens cracked while 50% of the abraded specimens cracked. Also, the time to failure for the tarnished specimens was longer than the single abraded specimen. Obviously, the small number of specimens prevents any statistically

significant conclusions; however, the resulting trend does appear to indicate that the results for the tarnished and abraded specimens are approximately the same. This conclusion is further substantiated by the lightly sensitized specimen test results where although 25% (1 of 4) of the tarnish specimens cracked while none of the three abraded specimens failed, the latter tests exposure period was only 141 days as opposed to 459 days for the tarnished specimens. Additional short term tests of highly stressed tarnished and abraded specimens in 0.2 ppm oxygen water produced no indications of IGSCC on any of the specimens. This implies again that there appears to be no significant difference in IGSCC response.

Ward, et.al.[2] performed laboratory investigations primarily designed to determine the effects of fluoride ion on the intergranular attack resistance of austenitic stainless steels. However, the results of their investigation do provide some data relevant to the present concern even though coated electrodes were not used for the DAEC repair. The tests consisted of four point bent beams with a uniform strain of approximately 2%. Most specimens were characterized by a transverse weld bead at the center. In the tests where the weld slag oxidation and welding fumes remained on the specimen surface, heavily furnace sensitized (10 to 24 hours at 621°C) Type 304 suffered from intergranular attack (IGA) after subsequent exposure for as long as 10 days in 82°C (180°F) water while heavily furnace sensitized Alloy 600 appeared to be completely resistant to attack. Annealed and welded specimens of either alloy did not suffer any significant attack.

JLR:cas/61D3

Pickett and Walker[3] of General Electric conducted studies which also demonstrated that post weld heat treat oxides had no effect on corrosion of Inconel 600 due to contaminations from flux and fumes from coated welding rods which contain fluorides in sufficient quantities to produce IGA of furnace sensitized Type 304. In this instance U-bends of furnace sensitized (621°C for 24 hours) Types 304, 304L, and 308L weld metal and Alloy 600 were contaminated with flux fumes by placing the specimens adjacent to an actual weld pass on a plate. The specimens were subsequently placed in 38 and 82°C (100 and 180°F) de-ionized water for exposure periods up to 30 days.

The results of this study indicated that although the surface oxide film from the sensitizing heat treatment appeared to accelerate IGA of flux contaminated Type 304, Alloy 600 was immune to this type of attack. Similarly, recent additional General Electric pipe test SCC studies[4] in 550°F oxygenated water have indicated no significant difference in the IGSCC response of Alloy 600 specimens with a post weld vessel heat treatment (PWVHT) film (621°C for 24 hours) as compared to as welded only specimens. This result occurred despite the fact that PWVHT sensitized the Alloy 600 microstructure. Therefore, the relatively thick surface oxide film as created by PWVHT clearly did not contribute to any premature IGSCC response in Alloy 600.

Discussion

Data from the open literature and recent General Electric studies indicate oxide films as produced by sensitizing heat treatments or welding fluxes have no significant effect on the IGSCC response of Alloy 600 although

it may have some minor effect on Type 304 stainless steel's IGSCC response. It is important to note that the thermally grown oxide film as produced by sensitizing heat treatments or welding is not the same as the passivation films present on corrosion resistant materials such as Alloy 600 and stainless steel. Whereas a film formed in dry air consists essentially of an anhydrous oxide, in the presence of water (ranging from condensed films deposited from humid atmospheres to bulk aqueous phases such as the BWR), the film on Fe-Ni-Cr alloys becomes a partially hydrated thin transparent layer.

It appears that the only effects the presence of the localized and isolated regions of oxide scale could have on the IGSCC response of Alloy 600 would be of a mechanical and not electrochemical nature. Even though it has been postulated that, depending on its porosity, the oxide scale could serve as a crevice in a worst case situation, the data presented above indicates that this does not occur. Therefore, in spite of the formation of the thermally grown porous oxide, it appears that the rate controlling step of the IGSCC process of Alloy 600 reverts back to that of a phase boundary reaction and therefore becomes independent of any oxide present.

Any dissolution of the surface oxide layer into the molten insert could lead to islands of oxide with adjacent chromium depleted regions in the weld root area. Such a condition would be similar to the chromium depleted grain boundary microstructure which is typical of mill annealed and welded Alloy 600. The chrome depletion on the grain

boundary is the more limiting condition since any crack path would tend to be intergranular. Therefore the existence of islands of oxide should not adversely affect the stress corrosion susceptibility of the Alloy 600 base or weld metal .

Another source of possible concern could be scale induced tensile stresses. The possible mechanism of stress generation could consist of epitaxial strain, oxide formation in cracks or grain boundaries (oxide wedging) and formation of high local stresses. Although the presence of these possible mechanisms could possibly contribute to the localized stress

state, the fact that these oxides are created at extremely high temperatures during welding and are probably stress relieved due to thermal effects with additional stress dissipation by plastic flow of the oxide, should reduce this potential concern to an insignificant level. It should also be noted that this effect has not been identified in this alloy system.[5]

Conclusions

From the preceding discussion the following conclusions are drawn concerning the presence of a welding oxide scale on the IGSCC propensities of Alloy 600:

1) Although laboratory data indicate that the IGSCC kinetics of furnace sensitized Type 304 may be somewhat affected by the presence of a thermally grown oxide film, Alloy 600 does not appear to have the same type of response.

2) No data has been identified which indicates that the presence of a thermally grown oxide film will adversely effect Alloy 600 IGSCC resistance.

3) Theoretically, the presence of a thermally grown oxide film on Alloy 600 should have no chemical effects on the passive film from which Alloy 600 IGSCC resistance is determined.

JLR:cas/61D6

4) The possibility of oxide mechanical effects such as oxide wedging is remote due to the thermal stress relief of the oxide during welding and cooling and the mechanical stress relief due to plastic flow of oxide which would also occur during the welding and cooling process.

JLR:cas/61D7

REFERENCES

1. Berry, W. E., White, E. L., and Boyd, W. K., "Stress Corrosion Cracking of Sensitized Stainless Steel in Oxygenated High Temperature Water," Corrosion, Vol. 29, No. 12, December 1973.

2. Ward, C. T., Mathis, D. L. and Staehle, R. W., "Intergranular Attack of Sensitized Austentic Stainless Steel by Water Containing Fluoride Ions," Corrosion, Vol. 25, No. 9, September 1969.

3. Pickett, A. E. and Walker, W. L., "Corrosive Effects of Coated Welding Electrode Flux and Fumes on Type 304 Stainless Steel," presented at NACE Western Region Conference, Los Angeles, CA, October 6-8, 1970.

4. Sauby, M. E., unpublished data.

5. Castle, J. E., "Discontinuous Oxide Films," Corrosion, Newres-Butterworths, London, 1976.

JLR:cas/61D8

Oxygen Level ppm	Stress Level	Degree of Sensitizat
100	3Sm	Light
100	3Sm	Heavy
100	2Sm	Light
100	2Sm	Heavy
100	Sm	Light
10	3Sm	Heavy
10	2Sm	Heavy
0.2	3Sm	Light
0.2	3Sm	Heavy
10 + 1F	2Sm	Light
10 + 10F	3Sm	Heavy
0.2	3Sm	Light
0.2	3Sm	Heavy

[1] N = no failure, and blank inc

JLR:cas/61E1

II.C STRESS AND FATIGUE EVALUATION

In the absence of a precise description of the weld root condition in the subject welds, stress and fatigue analyses were performed for a number of different assumed notch configurations as shown in Figures II.C-1 and II.C-2 for the safe end to piping weld (Weld #6) and the nozzle to safe end weld (Weld #2), respectively. The assumed notches range from Case A, which is a relatively shallow 0.015 inch semi-circular groove, through Case E, which is an extremely conservative, 10% of wall thickness cusp-shaped notch. Case F is the notch configuration judged to be representative of the worst root condition in any of the welds based on micro-densitometer mapping of the radiographs.

An additional conservatism is introduced in the analysis by the fact that in all cases the notches are assumed to exist continuously around the circumference of the welds (360°). The actual discontinuities on the radiographs were only a few inches long.

One of the major effects of the assumed notches is to introduce a stress concentration factor which amplifies the nominal stresses in the weld. Classical elastic stress concentration factors were determined for cases A through D and F (Ref. 1). Case E was treated as if it were the notch configuration which would exist at the root of a partial penetration weld, in which case the ASME Boiler and Pressure Vessel Code (Section III, Paragraph NB-3352.4 (d)) provides an empirically determined fatigue strength reduction factor of 4.0.

JLR:cas/61G1

A second effect of the assumed notches is to cause an increase in the primary, axial stress components due to assumed wall thinning. It is noteworthy that no wall thinning actually occurred in any of the welds because sufficient weld reinforcement is present at the weld outside diameters to more than compensate for the observed suckback condition at the weld inside diameters. Nevertheless, wall thinning was assumed to occur in proportion to the depth of the assumed notches, and the axial, primary stress components were scaled accordingly. This wall thinning assumption thus represents another conservatism in the analysis.

Stress report values for the various ASME Code Stress Categories at the appropriate weld locations were taken from Reference 2, and are listed in the first columns of Tables 1 and 2 for Weld #6 and Weld #2, respectively. The ASME Code allowable for each stress category is also tabulated. Note that, in every code category, the stresses reported in Reference 2 are substantially lower than the ASME Code Allowable. The remaining columns of Tables 1 and 2 list increases to the reported stress which account for the various assumed notch configurations as described above. In the primary membrane stress category, the governing stress component is hoop rather than axial, and thus no increase in stress occurs due to the assumed notches. In the other primary and secondary categories, some stress increase occurs, but is minor in comparison to the margins which exist between the stress report values and the allowable code limits. The only significant stress increase occurs in the alternating stress category because this stress category

reflects the notch stress concentration factors which are fairly high. Nevertheless, fatigue usage factors based on these increased alternating stress values are still below the ASME Code allowable of 1.0.

The bottom rows of Tables 1 and 2 provide estimates of the GE stress rule index for mitigation of stress corrosion concerns. A target value of 1.0 has been proposed by GE for sensitized stainless steel in the BWR environment and data were presented in Reference 3 which support this as a reasonable target value for inconel where crevice stress corrosion may be a concern. The assumed notches do raise the stress rule indices slightly above the target value of 1.0. While this is not viewed as a serious concern, the potential consequences of stress corrosion cracking propagating from an assumed notch are addressed in Section V. of this report.

In summary, a number of assumed notch configurations in DAEC recirculation replacement welds #2 and #6 were found to have a negligible effect on the stresses reported in the stress report in all major ASME Code stress categories. In all cases the stresses remain well below code limits.

JLR:cas/61G3

TABLE II.C-1

RESULTS OF STRESS AND FATIGUE EVALUATION OF
VARIOUS ASSUMED NOTCH CONFIGURATION IN PIPING TO SAFE-END WELD (WELD #6)

STRESS CATEGORY	STRESS REPORT VALUE	NOTCH CONFIGURATIONS						ALLOWABLE LIMIT
		A	B	C	D	E	F	
Primary Membrane (KSI)	11.91	11.91	11.91	11.91	11.91	11.91	11.91	Sm = 23.3
Primary Membrane (OD) + Bending (KSI) (Avg)	20.0	20.44	20.59	21.05	22.2	22.2	21.27	1.5 Sm = 35.0
Primary (w/ the bending)	70.6	70.76	70.81	70.97	71.4	71.4	70.89	-
+ Secondary Range (KSI) (w/o thermal bending)	18.7	18.86	18.91	19.07	19.5	19.5	18.99	3 Sm = 69.9
Stress Concentration Factor (Elastic)	1.0	2.93	2.90	2.83	3.3	4.0	2.02	-
(Plastic)	1.03	1.041	1.043	1.05	1.07	1.07	1.047	-
Alternating Stress (KSI)	50.9	142.83	141.53	139.55	166.5	201.63	99.4	-
Fatigue Usage Factor	0	.32	.31	0.31	.52	.86	0.129	1.0
GE Stress Rule Index Rule	0.96	1.18	1.18	1.18	1.27	1.38	1.06	1.0*

*Suggested Target Value for Mitigation of Potential Stress Corrosion Cracking Concerns.

JLR:cas/61H1

TABLE II.C-2

RESULTS OF STRESS AND FATIGUE EVALUATION OF
VARIOUS ASSUMED NOTCH CONFIGURATIONS IN SAFE-END TO NOZZLE WELD (WELD #2)

STRESS CATEGORY	STRESS REPORT VALUE	NOTCH CONFIGURATIONS						ALLOWABLE LIMIT
		A	B	C	D	E	F	
Primary Membrane (KSI)	8.1	8.1	8.1	8.1	8.1	8.1	8.1	Sm = 23.3
Primary Membrane (OD) + Bending (KSI) (Avg)	8.5	8.94	8.99	9.26	9.78	9.78	9.05	1.5 Sm = 35
Primary (w/ the bending)	20.6	20.74	20.79	21.06	21.58	21.58	20.85	35m = 69.9
+ Secondary Range (KSI) (w/o thermal bending)	-	-	-	-	-	-	-	
Stress Concentration Factor (Elastic)	1.0	3.1	2.9	2.8	3.3	4.0	2.1	-
(Plastic)	-	-	-	-	-	-	-	-
Alternating Stress (KSI)	13.2	41.03	38.49	37.59	45.12	54.58	21.78	-
Fatigue Usage Factor	0.0	0.00207	0.00151	0.00151	0.00443	0.0103	0	1.0
GE Stress Rule Index Rule	0.76	1.017	0.997	0.991	1.07	1.15	0.907	1.0*

*Suggested Target Value for Mitigation of Potential Stress Corrosion Cracking Concerns.
JLR:cas/61H2

REFERENCES

1. R. E. Peterson, Stress Concentration Design Factors, J. Wiley & Sons, 1953.

2. Stress Report for Recirculation Inlet Nozzle Safe-End Replacement at Duane Arnold Nuclear Plant, CBIN Contract No. 8-CN245, August, 1978.

3. Duane Arnold Energy Center Recirculation Inlet Safe-End Repair Program, Iowa Electric Light and Power Company, December 8, 1978.

JLR:cas/61G4

FIGURE II.C-1: Analyzed Notch Configurations at Root of Safe End to Piping Weld (Weld #6)

CASE	NOTCH CONFIGURATION	% OF WALL	STRESS CONC. FACTOR
A	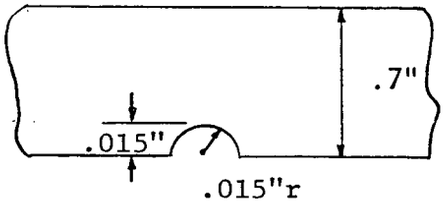	2.14%	2.93
B	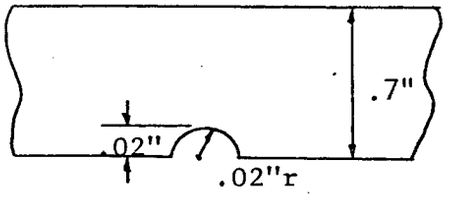	2.86%	2.90
C	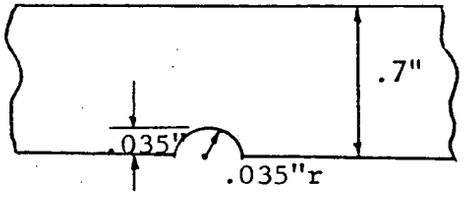	5%	2.83
D	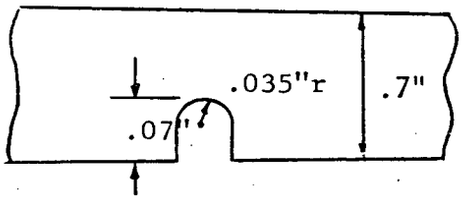	10%	3.3
E	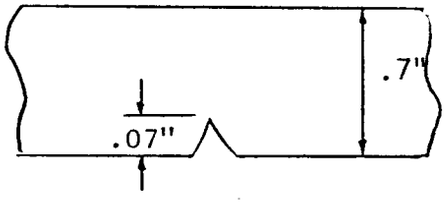	10%	4.0
F	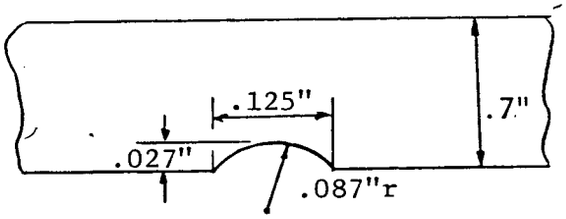	3.86%	2.02

FIGURE II.C-2: Analyzed Notch Configurations at Root of Nozzle to Safe End Weld (Weld #2)

CASE	NOTCH CONFIGURATION	% OF WALL	STRESS CONC. FACTOR
A	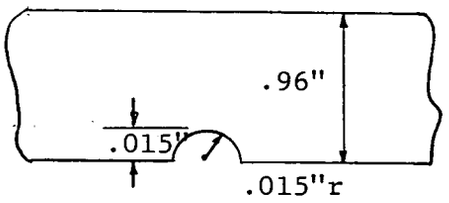	1.56%	3.1
B	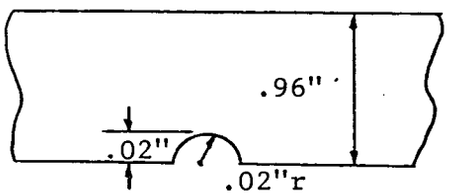	2.08%	2.9
C	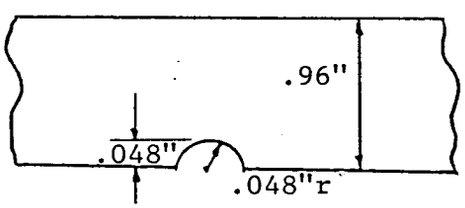	5%	2.8
D	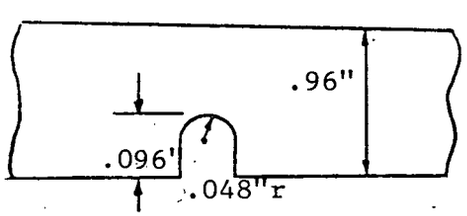	10%	3.3
E	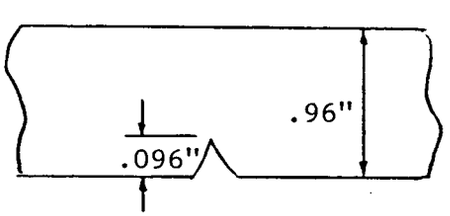	10%	4.0
F	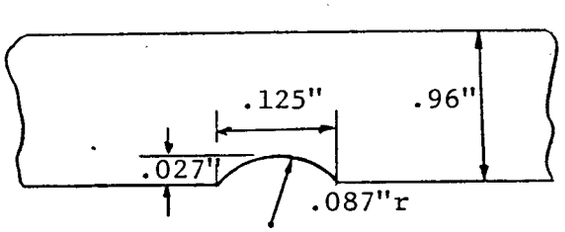	2.81%	2.1

II.D UT INSPECTABILITY OF WELDS WITH IRREGULAR CONTOURED ROOTS

The question has been raised as to the effect of irregular weld root configuration upon ultrasonic inservice examinations. Clearly the presence of such geometric reflectors as root concavity and drop through complicates the examination, but they need not destroy its effectiveness. These complex weld geometries only require that the preservice (baseline) examination data be reliable and complete. When the baseline data is adequate, then subsequent examinations are meaningful. In the case of the Duane Arnold Energy Center safe end repair welds, ultrasonic baseline data was recorded on strip charts. Every indication's amplitude, range, travel, and circumferential extent are shown on these charts. When similar inservice examination data is compared with the baseline, the recorded geometric reflectors will serve as reference points checking the reproducibility of the test. New indications, or significant changes in old indications, can readily be identified against this reference level background.

Performing and recording a detailed baseline of the replacement safe ends with the test sensitivity increased beyond ASME, Section XI requirements is expected to enable subsequent similar pressure boundary examinations of the safe ends to achieve a 10% detection level.

JLR:cas/61B13

chloride. Thus, it may not significantly accelerate propagation.

Although the presence of lead shortens the time to crack initiation in Alloy 600, this initiation time is still long relative to the time required to completely dissolve the lead smears. At the maximum BWR Coolant temperature of 546^{o}F, the shortest reported time to crack initiation is on the order of 24 weeks at an applied stress of 1.25σy. Although shorter times have been reported at higher temperatures, e.g. 4-6 weeks at 600-630^{o}F, these results are not directly relevant to the BWR case. Because of the short measured time required to completely dissolve the smears ($\leq$2 days), there should be no effect of these lead deposits on the stress corrosion crack initiation.

The only Alloy 600 components which could contain lead smears are located in the lower plenum area. The control rod drive stub tubes and attaching welds and the incore housing to vessel attachment welds (Figure III.D-1) are the only pressure boundary components made of Alloy 600 located in this area. During shutdown and normal operating conditions the component dead weight loads and system internal pressure loads result in stresses which are primarily compressive. These compressive stresses tend to reduce any overall tensile stresses which might be present due to weld residual stresses. The time dependence of any lead accelerated stress corrosion cracking has already been discussed. The combination, then, of the relatively short period of time that lead might be present on the pressure boundary components during the cleanup process and the

III.A RECOVERY OF NOZZLE B PLUG

After verification of flow blockage of N2B recirculation pipe by means of jet pump flow indications, a program was developed to determine what was causing the blockage and how the blockage would be removed. The following is a sequence of steps to date to implement the program:

1) A fiberscope was inserted into the 1" LPCI loop selection ΔP instrument line just below the riser elbow to observe possible blockage. A 70" fiberscope was inserted and six lead bricks of various sizes were found at the riser elbow inside the reactor wall. This discovery indicated that a lead plug was left in N2B after welding completion. See Figure III.A-1.

2) As flow blockage was assumed to be also in the rams head components of riser pipe N2B, the rams head and attached jet pump sections were removed. Lead bricks were observed to be lodged in #3 and #4 jet pump nozzle throats. Also, a portion of the lead plug canister backing plate was found lodged in one jet pump throat. This backing plate is shown in Figure III.A-1.

3) After the 2 ramshead components were removed, the lead plug canister wall was found lodged in the flow splitter casting at the top of the riser pipe. This canister wall is shown in Figure III.A-1.

JLR:cas/61B1

4) The lead brick-sheet metal retrieval program was developed to get the pieces out from the riser pipe from the reactor jet pump area. Special pliers operated by air cylinders were developed with various jaws in order to grab the brick in the riser elbow. Mockups were built to practice the retrieval techniques (procedures, tools, and remoteness) prior to the actual attempt in the reactor. By observing the remote operation with underwater TV, the six lead bricks were retrieved in about six hours and was considered to be very successful. The sheet metal canister was retrieved and found to be intact with the exception of some small tabs used to hold the backing plate in place. A total of 21 tabs were missing from the canister. The tabs are shown in Figure III.A-1.

5) A total of 3 lead bricks, 5 metal tabs, and a major portion of the backing plate were retrieved from the two rams head components.

6) An account of all components retrieved was performed and resulted in the following missing parts:

   a) a lead brick weighing 2 lbs, 3 oz. (This is brick #1 in Figure III.A-1.)

   b) 16 metal tabs measuring: ~1 " x 1 " x .015"

   c) A portion of the aluminum canister backing plate measuring 9.5" in diameter with a cord length of 5.25" and a thickness of 0.016".

JLR:cas/61B2

7) At the present time, a program has been developed to retrieve the missing lead brick from the bottom head area of the reactor. The program involves a fuel cell by fuel cell search of the vessel. The search is being conducted by completely disassembling all of the fuel cell components, using the underwater TV and reassemblying the cell if nothing is found and then proceeding to the next cell. A search pattern has been developed as being the most likely area to begin looking for the lead brick.

JLR:cas/61B3

ASSEMBLED CANISTER

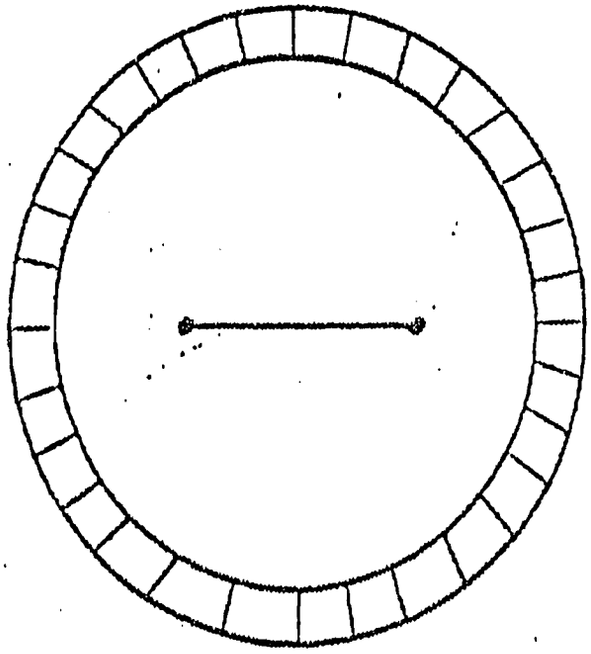

CANISTER SIDE

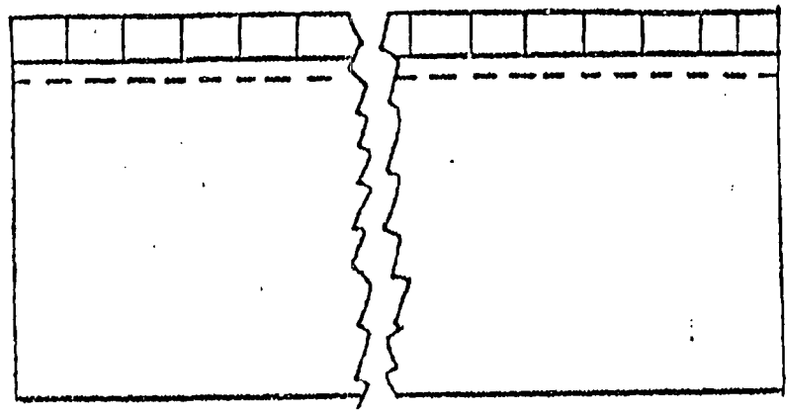

Note:
Canister Side 32" x 6" x 0.016"
Tabs rolled 1"
Tabs bent 0.75"

Aluminum Backing Plate
9 5/8" Dia.
0.016" thick
Holes spaced ~3-4 inches

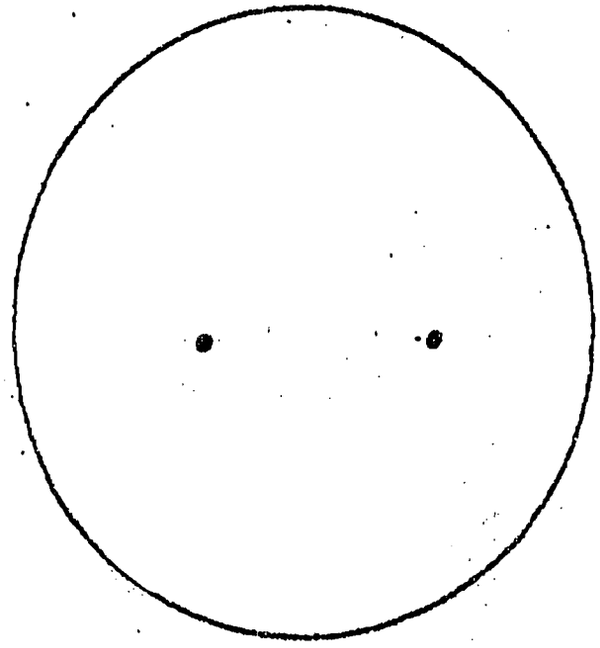

BACKING PLATE

SHIELD PLUG CANISTER

FIGURE III.A-1.a

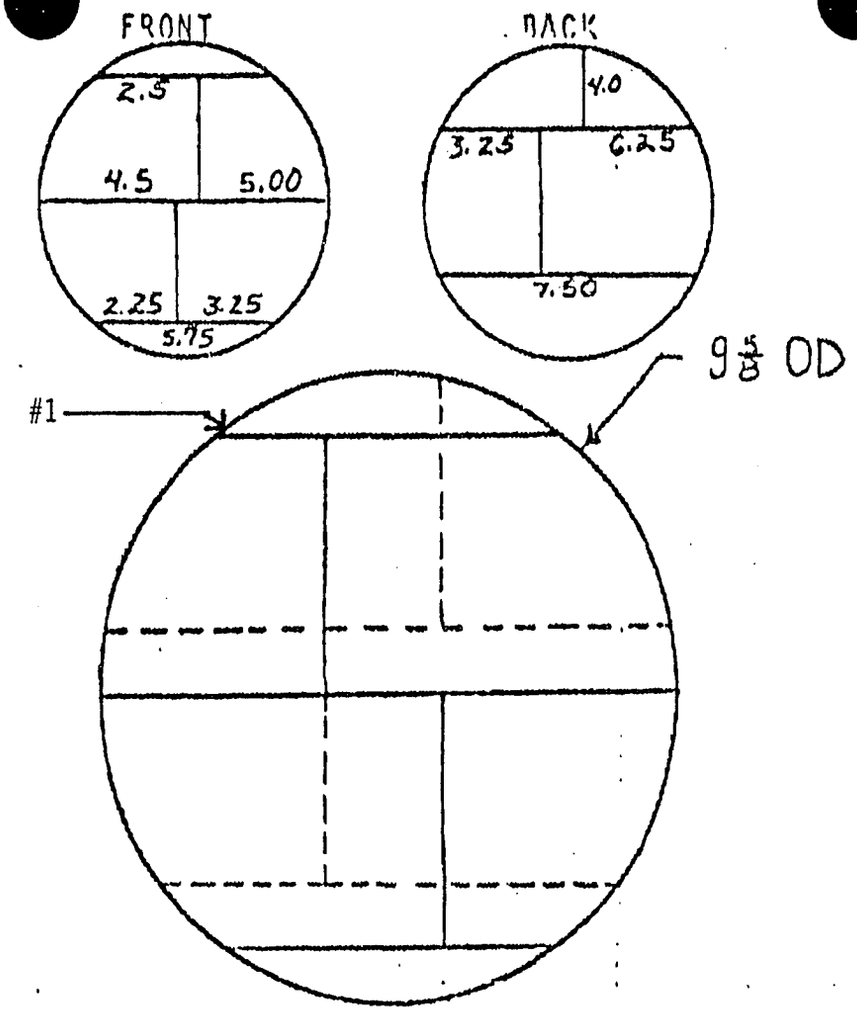

ASSEMBLED SHIELD PLUG.

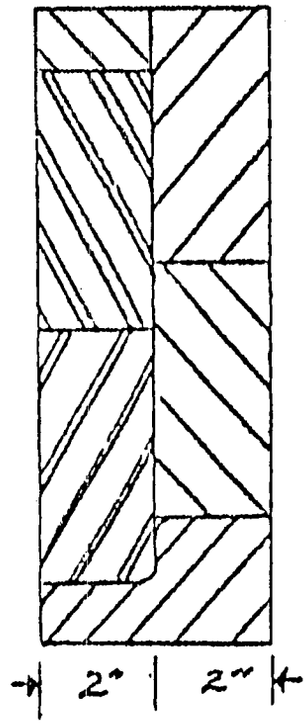

NOZZLE SHIELD PLUG

FIGURE III.A-1.b

III.B. RETRIEVAL OF OTHER SHIELD PLUGS

During the entire process of the safe-end-thermal sleeve adapter effort, lead plugs were inserted into the thermal sleeve riser pipe that remained attached to jet pump assemblies. These lead plugs consisted of ten various shaped bricks that formed a two layered circular array that would fit into a 10" canister. The purpose of the canister was to allow the bricks to be stacked into the thermal sleeve pipe without contacting the permanent Alloy 600 piping.

In order to insure that the lead bricks would not contact the inconel or stainless metal in the piping system, a metal trough was used to shield the pipes during assembly of each plug. A typical plug and canister assembly is shown in Figure III.A-1. Each plug has 2 holes drilled partially through the bricks to enhance the use of remote tools to install and remove the brick.

JLR:cas/61B4

III.C LEAD REMOVAL

1. Using Reactor Cleanup System

Laboratory testing in lead contaminated high temperature water has demonstrated that lead is soluble and can be transported by diffusion and flow. Lead has been found to precipitate in heat exchangers of flow autoclave facilities where lead testing was being performed (6). The rate of transport (or removal) of lead in water will be controlled by the flow and corrosion rate. The corrosion rate itself will be effected by temperature and the dissolved oxygen concentration in the water. Results of an unpublished experiment (6) in a deaerated all volatile treated (AVT) water at 288°C (550°F) yielded a corrosion rate of about 0.5 mils/yr. GE tests at 260°C (500°F) under conditions of aeration have indicated a rate of >10 mils/yr., a lead contaminated metal surface underflowing conditions could become clean in less than 2 days. The small amount of lead corrosion product involved should dissolve and be removed by the reactor cleanup system.

III.D LEAD STRESS CORROSION CRACKING

Since the early 1960's when researchers from the International Nickel Company (INCO) found lead deposits on laboratory samples tested in France by Coriou, lead has been suspect of causing accelerated cracking of stressed Ni-Cr-Fe Alloy 600 in high temperature water. Since that time, extensive laboratory testing has been performed not only by INCO (1, 2, 3), but also by Westinghouse (5) and others (6). The consensus of the investigators is that metallic lead or lead compounds can accelerate initiation of cracking of stressed Ni-base alloys in high temperature (288 - 332°C) water when present in high concentrations (near the solubility limit) (4). Ni-Cr-Fe Alloy 600 test samples exposed to water plus lead oxide at 332°C and stressed as low as 90 percent of yield have cracked in both the as received (mill annealed) and "sensitized" conditions (5). Cracking has been observed in both non-deaerated (1) and deaerated (2, 3, 5, 6) environments.

When Type 304 stainless steel was included in laboratory studies involving lead contamination it was generally found to be resistant to stress corrosion cracking (5). The literature does, however, contain one reported case of cracking of Type 304 stainless steel in an unaerated lead-contaminated water at 316°C (600°F) (2). In this reference, Flint and Weldon of INCO, Europe reported work performed in the INCO, U.S. laboratory where one of seven highly stressed "furnace sensitized" U-bend specimens developed intergranular cracking (6). In the same test, two as received (mill annealed) and one solution annealed U-bend specimens of Type 304 stainless steel did not crack (6).

JLR:cas/61C1

Based on the literature, the concern for lead induced stress corrosion cracking of Ni-Cr-Fe Alloy 600 is significantly greater than for Type 304 stainless steel. However, the literature does not give a clear indication of the critical concentration of lead required for accelerated stress corrosion cracking. Most laboratory studies were ferformed under conditions which wuld develop a concentration of the lead or lead compound approaching the solubility. The solubility of lead in water under reactor conditions has not been established. The only clue to the solubility of lead in high temperature water was an unpublished experiment performed at the INCO U.S. laboratory (6) where 280 ppm of lead was analyzed in water sampled from a 316^{o}C autoclave containing 10 grams of lead powder. This relatively high dissolved lead condition is known to crack Alloy 600, but the lower threshold concentration of lead to accelerate cracking still remains unknown. As a worst case, the threshold concentration could be speculated to be equivalent to that of chloride ion where concentrations in the low ppm range appear to accelerate cracking of stainless steel at BWR type dissolved oxygen levels.

Discussion

Based on the available data (all obtained on relatively small samples), it can be concluded that dissolved lead accelerates Alloy 600 SCC initiation kinetics. However, no data are published indicating any adverse effect of dissolved lead on crack propagation rate. Since lead probably goes into solution as a positive ion, it would not be expected to migrate to the positively charged crack tip as is the case with

relatively low tensile stresses in these components would result in little or no impact on their stress corrosion susceptibility.

As noted above, the potential for stress corrosion cracking in Alloy 600 increases significantly with increasing temperatures. There have been no reported occurrences of Alloy 600 SCC in oxygenerated water (with or without lead present) at temperatures less than about 550°F. In deaerated water containing LiOH, a lower cracking temperature of ~425°F was reported for the Agesta reactor in Sweden[1]. Because of the steep temperature dependency of cracking, the low temperature ($\leq$ 212°F) operation of the Duane Arnold Reactor for about 36 hours following the lead brick injection should have no effect on SCC crack initiation. Further, the air saturated conditions (~8 ppm O_2) expected during subsequent shutdown/startup conditions, while increasing the oxygen content of the water, would not be expected to effect the stress corrosion response during this period of time since temperatures are low. Once the temperature of the plant is increased above about 300°F, the oxygen level in the water would reduce to the normal BWR environment (~0.2 ppm O_2).

Because of the low measured weight of lead associated with the smears (about 1.5 mg/cm^2), the actual lead concentration in the reactor pressure vessel coolant will be very low even if dissolution were to occur instantly. This concentration can be approximated from the area coverage of the smears as estimated from the TV video tape examination of the inside of the jet pump riser containing the bulk of the smears. For the estimated

value of 1% area coverage, there will be ~0.5 gms of lead within the vessel. This amount, when dissolved into the ~4.5×10^5 lbs of primary coolant, will result in a concentration of about 2 ppb. Actually, since the lead dissolution will occur slowly over 1-2 day period, the reactor water cleanup system should remove most of the lead before total dissolution of the deposits occur. Thus, the actual lead concentration at any given time resulting from the smears should be significantly less than 1 ppb.

At this low level, there is no expected effect of the lead on the general corrosion or stress corrosion response of the vessel internals and the core components indlucing the Zircaloy clad fuel and the fuel channels.

REFERENCES

1. H. R. Copson and S. W. Dean, "Effects of Contaminants on Resistance to Stress Corrosion Cracking of Ni-Cr Alloy 600 In Pressurized Water," Corrosion, Vol. 21, P. 1 (1965).

2. G. N. Flint, and B. A. Weldon, "Some Investigations Into the Stress Corrosion Behavior of Fe-Ni-Cr Alloys In High Temperature Water," International Nickel France, E.D.F. Direction des E'tudes et Recherches, Ermenonville - 13 au 17 Mars 1972.

3. H. R. Copson, D. van Rooyen, and A. R. McIlree, "Stress Corrosion Behavior of Ni-Cr-Fe Alloys in High Temperature Aqueous Solutions," paper presented at 5th International Congress on Metallic Corrosion, Tokyo, Japan, 1972, NACE, Houston, Texas, p.p. 376-379 (1974).

4. D. van Rooyen, "Review of the Stress Corrosion Cracking of Inconel 600," Corrosion, Vol. 31, p. 327 (1975).

5. I. L. Wilson, F. W. Dement, and R. G. Aspden, "Stress Corrosion Studies on Some Stainless Steels in Elevated Temperature Aqueous Environments," Corrosion, Vol. 34, p. 311 (1978).

6. Private communications.

JLR:cas/61C5

7. R. L. Cowan and G. M. Gordon, "Intergranular Stress Corrosion Cracking and Grain Boundary Composition of Fe-Ni-Cr Alloys," Stress Corrosion Cracking and Hydrogen Embrittlement of Iron Base Alloys, Conference at UNIEUX-Firming, France, June 12-16, 1973. Volume published 1977 by NACE, Houston, Texas.

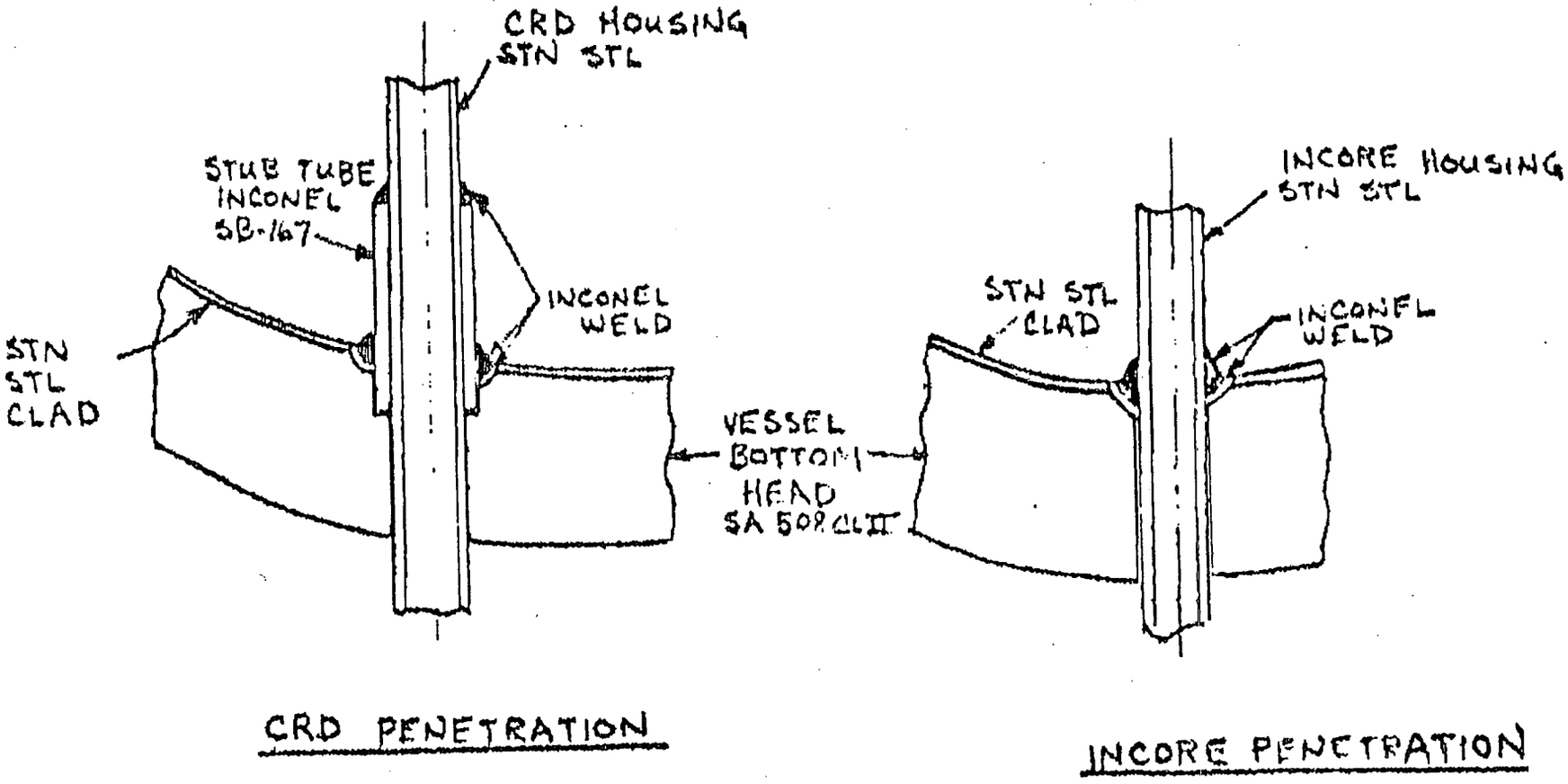

FIGURE III.D-1

IV. LOOSE PARTS ANALYSIS

A. Introduction

After completion of the recirculation inlet safe end repair at the Duane Arnold Energy Center (DAEC) but prior to going to power, it was discovered that some items had been inadvertently left in reactor pressure vessel (RPV). Recovery operations are continuing. This analysis shows that the presence of lost parts in the DAEC reactor pressure vessel (RPV) will not compromise safe reactor operation. A probablistic evaluation of the potential fuel bundle flow blockage is presented for information.

B. Lost Parts Description

The following parts are believed to be in the reactor vessel:

a) A piece of aluminum which was torn off the bottom of the protective canister. The piece has the shape of a segment of a circle of diameter 9.75" with a chord length of 5.25" and a thickness of 0.016". The precise aluminum alloy from which the piece was made is not known.

b) Sixteen (16) small carbon steel tabs which broke off from the protective canister. The tabs range in size from 3/4" x 3/4" to 1" x 1" and are 0.015" thick.

JLR:cas/61A1

All missing parts were either dropped into the jet pump diffuser or were left in the jet pump riser and were dislodged by flowing water into the diffuser. Thus, all parts are believed to be located in the bottom head of the RPV.

C. Safety Concerns

The following safety concerns are addressed in the safety analysis:

1) The potential for interference with control rod operation.

2) The potential for fuel bundle flow blockage and subsequent fuel damage.

3) The potential for corrosion or other chemical action to reactor materials.

D. Safety Evaluation

The potential for the lost parts identified in Section IV.B to cause the safety concerns identified in Section IV.C is addressed in this section. The effect of these safety concerns on safe reactor operation is also addressed.

D.1. Piece of Aluminum

Since the piece of aluminum is believed to be in the lower head of the PRV, it cannot have any effect on control rod motion. Aluminum will corrode very rapidly at BWR rated conditions. The specific corrosion rate is dependent on the alloy of aluminum involved. Even if located elsewhere, it will not be a problem.

Another piece of the bottom of the same protective canister will be put into an autoclave at reactor conditions to determine the time required for the aluminum to dissolve. The reactor can then be brought to 100 psi and 550^{o}F at a power level of less than or equal to 0.6 megawatts thermal per fuel bundle for the time required for the aluminum to dissolve. Fuel damage will not occur if the power in each fuel bundle is less than or equal to 0.6 megawatts thermal.

The small amount of aluminum will not cause any adverse chemical activity or corrosion to any reactor material.

D.2 Small Metal Tabs

Any missing tabs remaining in the inlet recirculation piping would be carried by the recirculation flow through the jet pump diffuser. The flow enters into the reactor vessel lower plenum. The lower

core support plate serves to channel the flow through the fuel support piece orifices past the fuel rods. All other potential core plate flow paths to the upper core region are plugged or have restrictive clearances which would prevent any of the missing tabs from leaving the lower plenum area.

Therefore, tabs exiting the lower plenum have to proceed with the flow around the guide tubes to the area of the fuel channel support pieces. Since they cannot pass through the fuel assembly lower tie plate, they cannot reach the upper core region to cause interference with control rod operation or any other reactor internal component parts.

The tabs are carbon steel, therefore, they will not corrode away for a long time. Any missing tabs trapped in the lower plenum will not cause any adverse chemical activity or corrosion of any reactor material.

The potential for fuel assembly flow blockage must be evaluated. There are three different fuel orifice sizes in the DAEC reactor. Figures IV-1 and IV-2 show the two orifice configurations and the three orifice diameters.

The largest tab is 1" x 1". Thus, all tabs will pass through either a central zone orifice (diameter 2.090") or a peripheral zone orifice (diameter 1.433"). The tabs are too large to pass through the fuel assembly lower tie plate. Thus if a tab passed through an orifice it would remain in the orificed fuel support. If all sixteen tabs came to rest against one fuel assembly lower tie plate, they would block approximately 66% of the flow area. Based on reference 1 a flow blockage of at least 79% is required to cause boiling transition. Thus the tabs are of no safety concern to the central zone or the peripheral zone fuel bundles.

The orifice diameter of the peripheral fuel bundles (Figure IV-2) is 1.225". A metal tab .87" x .87" could not pass through this orifice if the tabs were oriented adversely. If the size distribution of the lost tabs is the same as the tabs that were available for measurement, 46% of the tabs would pass through the orifice.

A statistical analysis was performed to determine the probability of peripheral orifice blockage due to the tabs. The following assumptions were used:

a) All tabs go to a fuel assembly.

b) The probability of a tab going to any peripheral fuel assembly is equal to that for any other fuel assembly; given that no flow blockage exist.

The binomial distribution (reference 1) was used in the following manner to estimate the probability of tabs reaching a peripheral fuel assembly:

$$\underline{P} = F \frac{N!}{X! \quad (N-X)!} \underline{P}^{X} \ (1-\underline{P})^{N-X}$$

$\underline{P}$ = probability of X or more tabs reaching a peripheral fuel assembly

F = number of peripheral fuel assemblies

N = number of tabs that are large enough that they may not pass through the orifice

X = number of tabs reaching the peripheral fuel assembly

p = probability of any particular tab reaching any particular peripheral fuel assembly equals one over the total number of fuel assemblies.

JLR:cas/61A5

$$F = 12$$

$$P = \frac{1}{368}$$

N was estimated at the 95% confidence level from the size distribution of the recovered tabs to be no more than 13 out of 16.

Two additional factors must be included to determine the probability of orifice blockage. They are: the probability (P_1) of a tab that is large enough to cause blockage to actually cause blockage, and the conditional probabilities of a second (P_2) and third (P_3) tab reaching a partially blocked orifice. Figure IV-3 shows how P_1 was estimated to be .09. P_2 was estimated to be .4 and P_3 to be .2 based on the flow reduction caused by the orifice blockage of other tabs. That is, the first tab will reduce (reference 1) the flow to 40% of its original value. Thus the driving force is reduced to 40% of its original value. Similarly, two tabs will reduce the driving force to 20% of its original value.

Thus the probability of one tab reaching any peripheral bundle and causing orifice blockage is

$$P_1^* = (.09)\ (12)\ \frac{13\ !}{1!\quad (12!)}\ \left(\frac{1}{368}\right)\quad \left(1 - \frac{1}{368}\right)^{12}$$

$$= .04$$

JLR:cas/61A6

The probability of two tabs reaching the same peripheral fuel assembly and causing orifice blockage is conservatively given by:

$$P_2^* = (.09)\ (12)\ \frac{13!}{2!\ (11!)}\ \left(\frac{1}{368}\right)^2 (.4)\ \left(1 - \frac{1}{368}\right)^{11}$$

$$= .00024$$

The probability of three tabs reaching the same peripheral fuel assembly and causing orifice blockage is conservatively given by:

$$P_3^* = (.09)\ (12)\ \frac{13!}{3!\ 10!}\ \left(\frac{1}{368}\right)^3 (.4)(.2)\ \left(1 - \frac{1}{368}\right)^{10}$$

$$= 0.0000005$$

The maximum possible orifice area blockage due to one tab is 81% of the flow area. Reference 1 states that 79% blockage will not result in boiling transition even for a central zone fuel assembly. Because the peripheral fuel assemblies are low power bundles, the flow blockage required for boiling transition is greater than 79%. It is estimated that this value is 83% - 100%. Thus, 81% blockage will not lead to boiling transition and the low probability of orifice blockage due to two or more tabs will probably not lead to boiling transition. In any case, safety consequences more severe than those described in Reference 1 would not be expected. In addition, based on reference 1, fuel damage is never anticipated for blockage less than 95%.

JLR:cas/61A7

E. Conclusions and Recommendations

This safety analysis has shown that no corrosion or other chemical action to reactor materials is expected to occur due to the lost parts. In addition, no adverse effect on reactor water chemistry is expected.

It has also been shown that there is no possibility of interference with control rod motion.

The possibility of fuel bundle damage due to the piece of aluminum can be eliminated if the reactor is operated at $\geq$ 550°F for a period of time based on future autoclave tests at a power level of less than or equal to 0.6 megawatts thermal per fuel assembly.

Flow blockage due to the carbon steel tabs has been shown to be of no safety consequence.

Therefore, if the above recommendation is followed, it is concluded that the presence of the lost parts in DAEC reactor vessel will not compromise safe reactor operation.

F. References

1. NEDO-10174, Revision 1, Consequences of a Postulated Flow Blockage Incident in a Boiling Water Reactor," October 1977.

JLR:cas/61A9

2. Neville and Kennedy, "Basic Statistical Methods For Engineers And Scientists"; International Text Book Company, 1964.

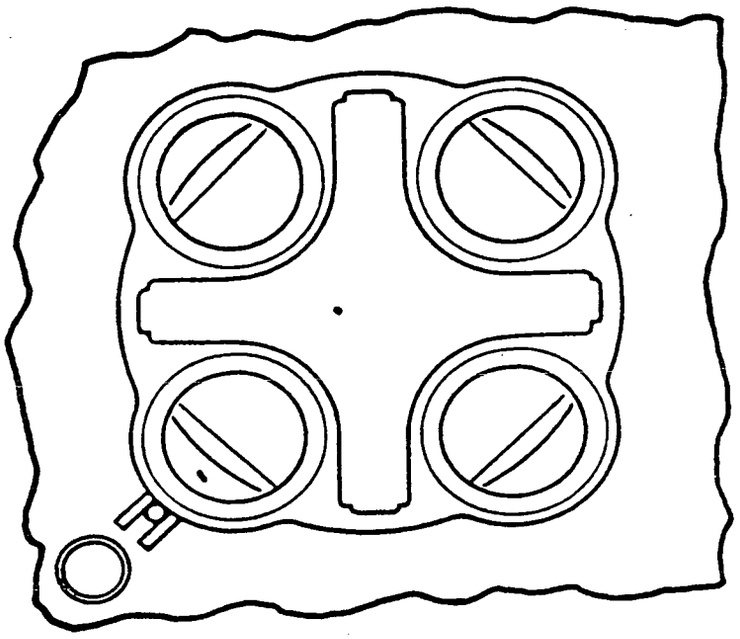

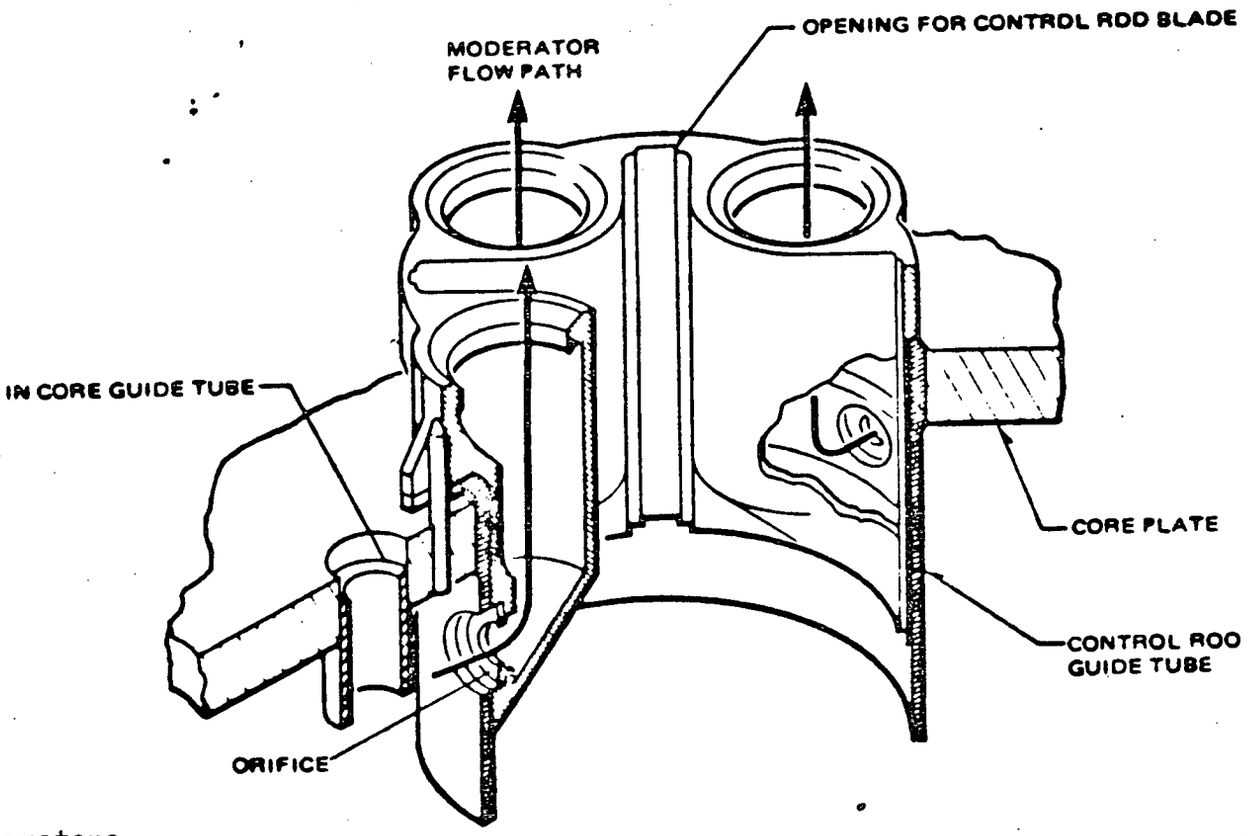

Diameters
Central Zone = 2.090
Peripheral Zone = 1.433

Figure IV-1
Orificed Fuel Support

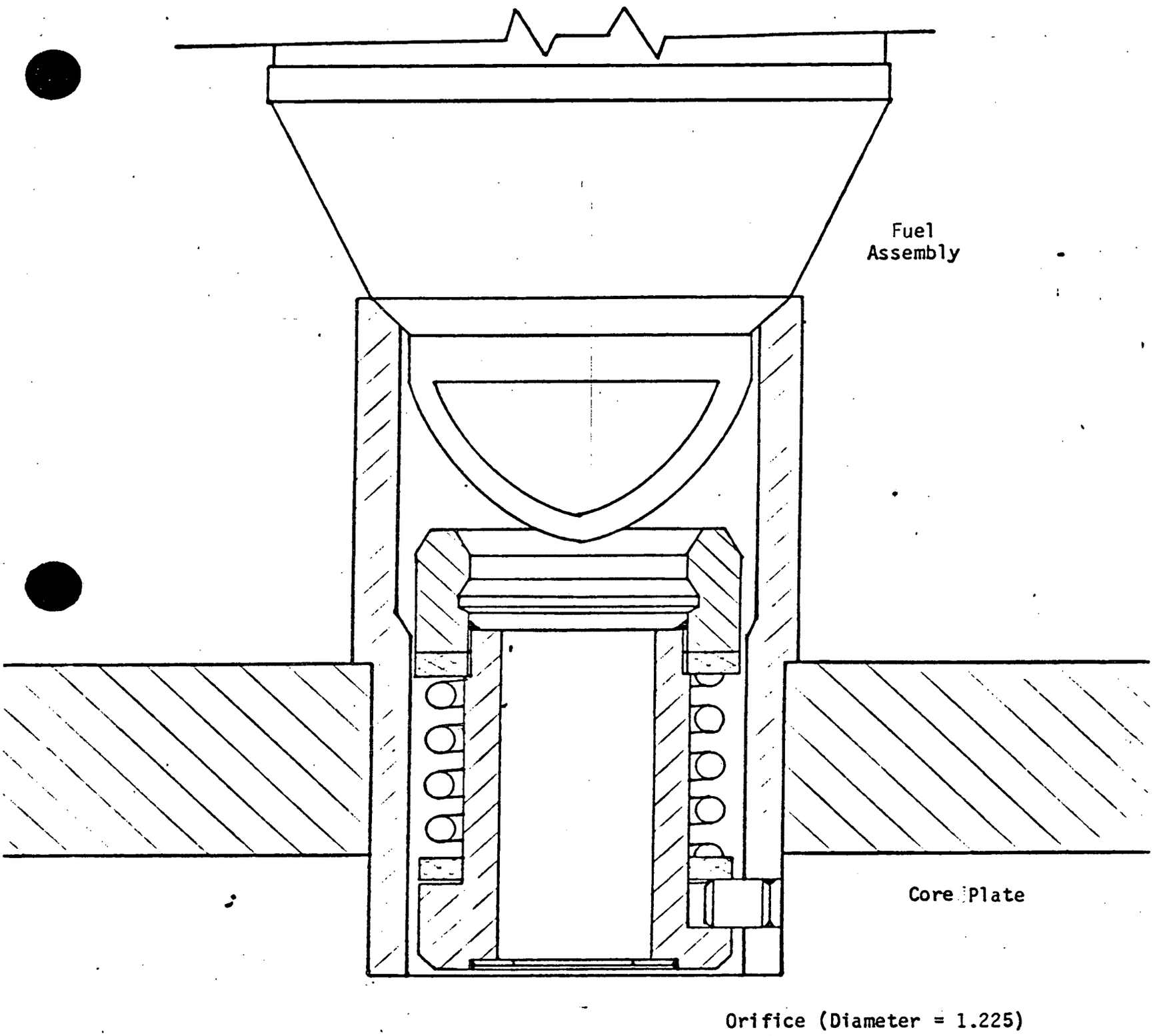

Figure IV-2

Peripheral Fuel Support Assembly

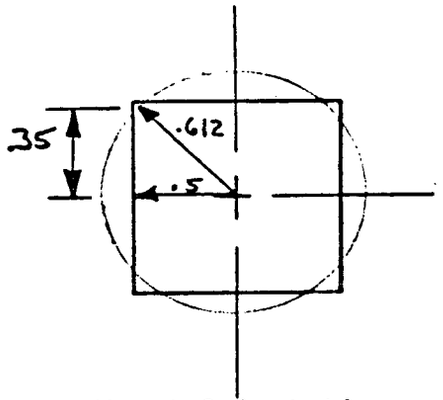

Orifice Diameter = 1.225

Largest Tab = 1" x 1"

Worst Orientation
with a 1" x 1" tab
Maximum blockage = 81%

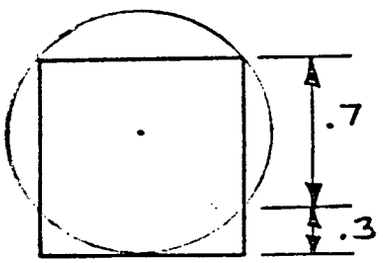

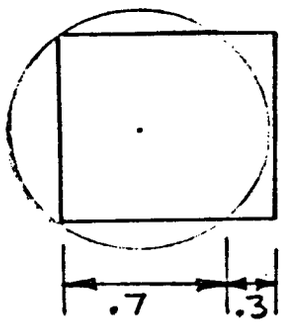

Limiting orientation which can cause blockage.
The probability of a 1" x 1" tab causing blockage
is less than or equal to $\frac{.3}{1.0}$ $\frac{.3}{1.0}$ = .09

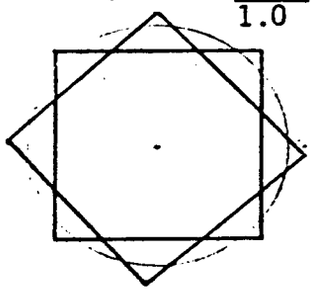

Worst orientation with 2 tabs.

Maximum possible blockage = 90%

Probability of orifice blockage

Figure IV-3

V. STRESS CORROSION CRACK PROPAGATION ANALYSIS

A. Stress Corrosion Crack Propagation Rate for Alloy 600 in BWR Primary Coolant Environment

The weld radiographic indications discussed in Section II of this report are believed to represent smooth, non-crevice-like root concavity conditions. Nevertheless, a conservative crack propagation prediction has been performed by assuming that a stress concentrator similar to the cusp identified in Figures II.C-1 and II.C-2 exists for welds #2 and #6 in the replacement safe ends, and that the cusp acts as a creviced crack from which stress corrosion crack propagation initiates immediately.

In order to perform a crack propagation analysis under this conservative set of assumptions, the appropriate environmental crack growth rate law must be determined. A significant amount of experimental activity has been directed at identification of the critical stress intensity for stress corrosion crack initiation and propagation and its rate dependence both for Type 304 stainless steel and for Alloy 600 in BWR environments by General Electric, the Electric Power Research Institute and the Department of Energy. One of the earlier programs addressing this question was the Atomic Energy Commission - General Electric Project Agreement 37 begun in the early 1960's, in which the

crack initiation and crack propagation behavior of annealed and sensitized Types 304ss, 304Lss, Alloy 600 and A516 carbon steel were investigated in the primary water environment of an operating BWR (Dresden 1). A summary of the stainless steel crack propagation data from this program is given in Reference V.A-1. Among the specimens tested in that program were fracture mechanics specimens of each of the alloys which were precracked (and therefore creviced), bolt loaded to high initial stress intensities (25 and 50 ksi$\sqrt{\text{in}}$) and exposed to the primary reactor water environment under constant loading for up to 7,000 hours.

Following the reactor exposure the stainless steel and Alloy 600 specimens were sectioned and examined for evidence of crack extension. Significant crack extension was observed for the furnace sensitized specimens of both Type 304ss and Alloy 600 at both stress intensities. An average crack propagation rate was determined for each specimen and is plotted versus the start-of-test stress intensity factor in Figure V.A-1. Note that the Type 304ss and Alloy 600 furnace sensitized crack propagation rates are nearly identical. (Due to the constant displacement nature of the bolt loaded experiments, some reduction in stress intensity factor is expected as the crack propagates. This effect is considered negligible, however, since the measured amounts of crack growth in the experiments were relatively small in comparison to specimen sizes.)

Similar static fracture mechanics testing was performed at General Electric on Type 304ss specimens having the same specimen configuration and heat treatment condition in air saturated water (8 ppm oxygen). These results are also presented in Figure V.A-1. The crack growth rates in Figure V.A-1 are approximately one order of magnitude greater in high oxygen as compared to the low oxygen tests. This result is consistent with other General Electric stress corrosion cracking data for sensitized Type 304ss where an order of magnitude increase in stress corrosion cracking time to failure has been observed for laboratory coupons tested in a low oxygen (0.2 ppm) environment as compared to coupons tested in a high oxygen environment (8 ppm) (Ref. V.A-2). A curve drawn through the high oxygen data points in Figure V.A-1 and a parallel curve through the highest growth rate low oxygen data point produces a crack growth rate law for Type 304ss and Alloy 600 in a low oxygen environment of:

$$\frac{da}{dt} = 3.66 \times 10^{-7} (K)^{0.835} \qquad \text{(Equation 1)}$$

Where: a = crack length

t = time in hours

K = stress intensity in Ksi$\sqrt{in}$

On the other hand, if one draws a best fit growth rate curve through the low oxygen data alone, ignoring the high oxygen data, the growth rate law for these alloys in low oxygen BWR water becomes:

$$\frac{da}{dt} = 5.17 \times 10^{-9} (K)^{1.935} \qquad \text{(Equation 2)}$$

Where a, t and K are as above.

These two crack growth laws, which appear to bound the stress corrosion cracking crack growth behavior of creviced Alloy 600 in BWR water, are used in the stress corrosion crack propagation analyses of the DAEC recirculation safe-end welds, which follow.

REFERENCES

1. Kass, J.N. and Wettstein, D.A., "Alternate Alloy for BWR Pipe Applications - Second Quarterly Progress Report," EPRI Contract RP968, General Electric Co. NEDC-23750-2, March 1978.
2. Clark, W. L. and Gordon, G. M, "Investigation of Stress Corrosion Cracking Susceptibility of Fe-Ni-Cr Alloys in Nuclear Reactor Water Environments," Corrosion 29, No. 1, (January 1973).

FIGURE V.A-1: Stress Corrosion Crack Growth Rates for Type 304 Stainless Steel and Alloy 600 in High Purity Water at 550°F.

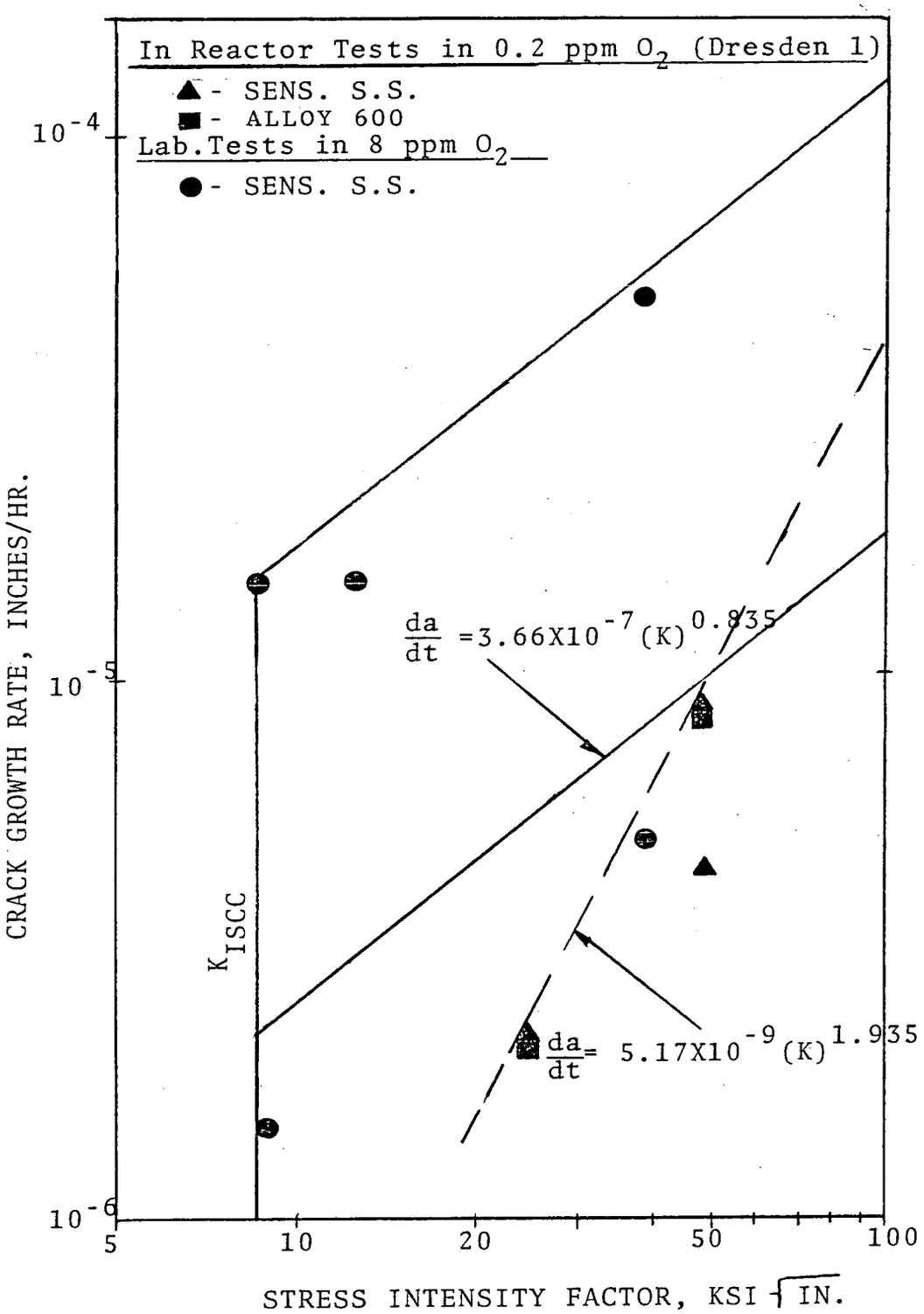

B. Stress Intensity and Crack Propagation Calculations

In order to perform a conservative stress corrosion crack growth life prediction for the original and replacement DAEC safe end welds, the axial components of sustained primary, secondary, peak and residual stresses must be determined and an initial crack depth assumed. The primary, and primary plus secondary plus peak stresses (both ID and through-wall) were taken from the stress report (Ref. II.C-2) and are presented for welds #2 and #6 of the replacement safe end and for the failure location of the original safe end in Figures V.B-1 and V.B-2. Through thickness residual stresses were estimated for the replacement safe end welds #2 and #6 from an Argonne National Laboratory Type 304ss residual stress program for 4-inch and 26-inch diameter schedule 80 Type 304 stainless steel butt welds (Ref. V.B-1). A Battelle Memorial Laboratory residual stress analysis for the original DAEC safe end design was used to describe the through-thickness residual stress for that design (Ref. V.B-2). The resulting residual stress distributions are given in Figure V.B-3. Since the 4-inch residual stres results taken from Figure V.B-3 are more tensile than the 26-inch results near the ID surface (and therefore more conservative), the 4-inch results have been used for the residual stress estimate for the replacement safe end welds.

Calculation of the through thickness stress corrosion crack growth was performed using a linear elastic fracture mechanics approach in which the stress distributions are curve-fit by a

third order polynominal and the stress intensity factor for the appropriate crack and component geometry is determined by applying appropriate magnification factors to the coefficients of the polynominal. Crack growth rate is then determined through integration of the appropriate crack growth law. For any stress distribution across a component wall thickness, a least square polynominal curve fitting routine is employed to obtain a third order equation of the form:

$$\sigma(x) = A_o + A_1 x + A_2 x^2 + A_3 x^3$$

where: $\sigma(x)$ = the stress at a point x through the thickness

x = fracton of thickness as measured from the ID surface

A_i = appropriate curve fit constants

Using the principle of superposition and the above stress equation, stress intensity factors for the specific crack model are generated for the constant, linear, quadratic and cubic stress terms. The resulting stress intensity factor is obtained by the following equation:

$$K = \sqrt{\pi a}\left(A_o F_1 + \frac{2a}{\pi} A_1 F_2 + \frac{a^2}{2} A_2 F_3 + \frac{4a^3}{\pi} A_3 F_4\right)$$

where: K = stress intensity factor

a = crack depth

F_1, F_2, $F_3 + F_4$ = Magnification factors for specific crack geometry being analyzed

JLR:cas/61I5

Stress corrosion crack propagation is then evaluated by numerical integration of the stress corrosion crack growth law:

$$\frac{da}{dt} = A\ (K)^n$$

where:

A and n are constants dependent on the stress corrosion cracking behavior of the material.

Using the stress distributions for the original safe end and the replacement safe-end welds #2 and #6, stress intensity factor versus crack depth was developed for each weld, and is presented in Figure V.B-4. What remains then is to utilize the stress corrosion crack growth laws developed in Section V.A for creviced, furnace sensitized Alloy 600 and determine conservative lifetimes for each weld.

Using Equation (1) from Section V.A

$$\frac{da}{dt} = 3.66 \times 10^{-7}\ (K)^{0.835}$$

and assuming an initial crack depth of 5% of the original safe end wall thickness, the crack depths for each of the weld designs as a function of time are as presented in Figure V.B-5. In this case for the original safe-end at the failure location, a 360^o crack averaging 70% of the wall thickness would develop in 3.5 years. For welds #2 and #6 of the replacement safe-end, the crack depths are less than 30% and 40% respectively in the equivalent time interval.

Alternatively, applying Equation 2 of Section V.A as the appropriate stress corrosion crack growth law

$$\frac{da}{dt} = 5.17 \times 10^{-9} (K)^{1.935}$$

and assuming an initial crack depth of 5% of the original safe end wall thickness, the crack depths for each of the weld designs as a function of time are as presented in Figure V.B-6. In this case, a crack will propagate to 70% of the wall thickness of the original safe end design in less than two years, while for welds #2 and #6 of the replacement safe end design, the crack depth is less than 20% of the wall even after three years.

JLR:cas/6117

REFERENCES

1. "Corrosion Studies of Nuclear Piping in BWR Environments," Argonne National Laboratories Quarterly Reports to the Electric Power Research Institute, Contract 31-109-38-3138L.

2. Battelle Memorial Institute Residual Stress Report to Iowa Electric - DAEC Original Design.

JLR:cas/61I8

FIGURE V.B-1: Primary Stresses for Original and Replacement DAEC Safe End Welds.

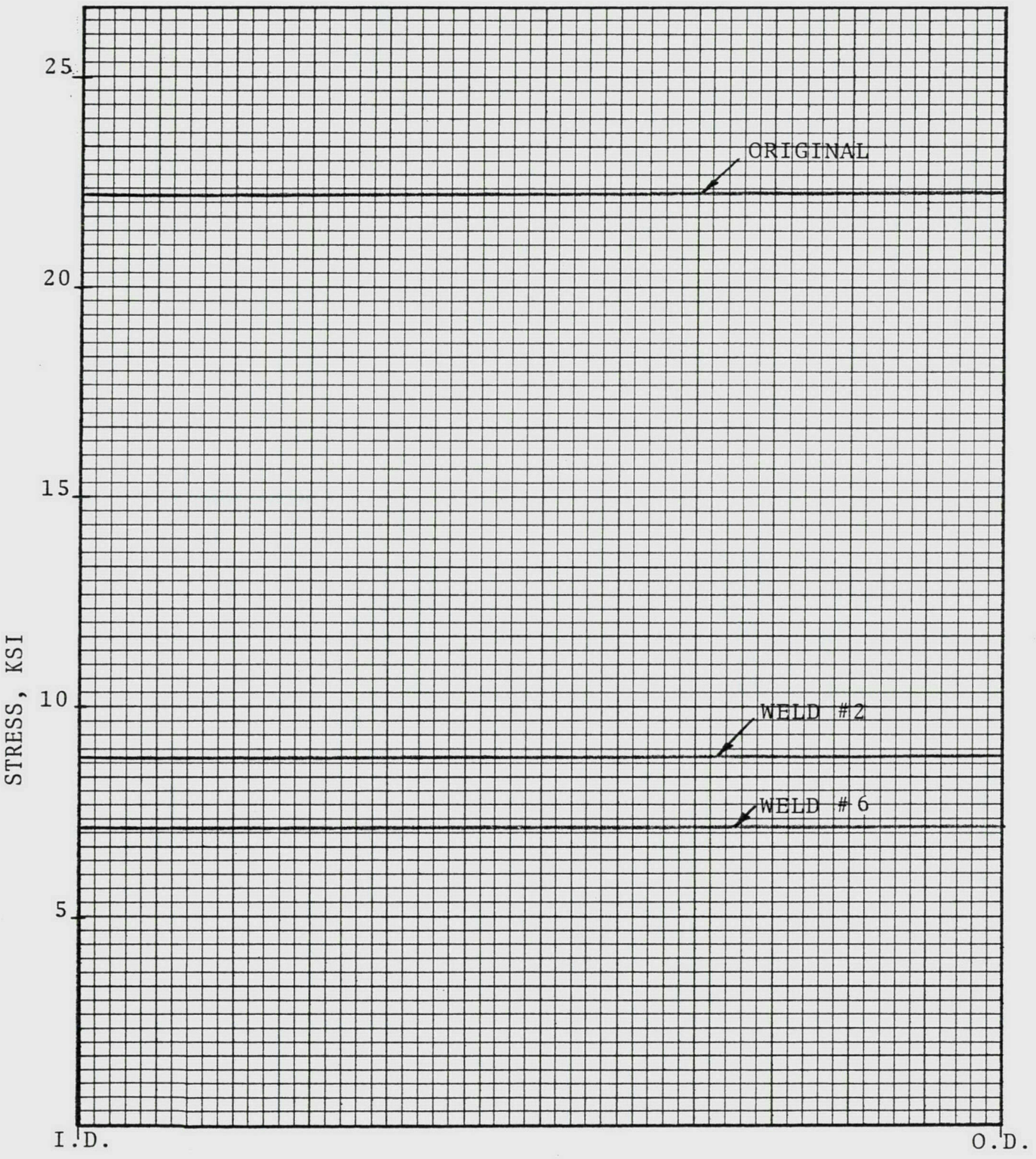

FIGURE V.B-2: Primary And Secondary Plus Peak Stresses for Original and Replacement DAEC Safe End Welds

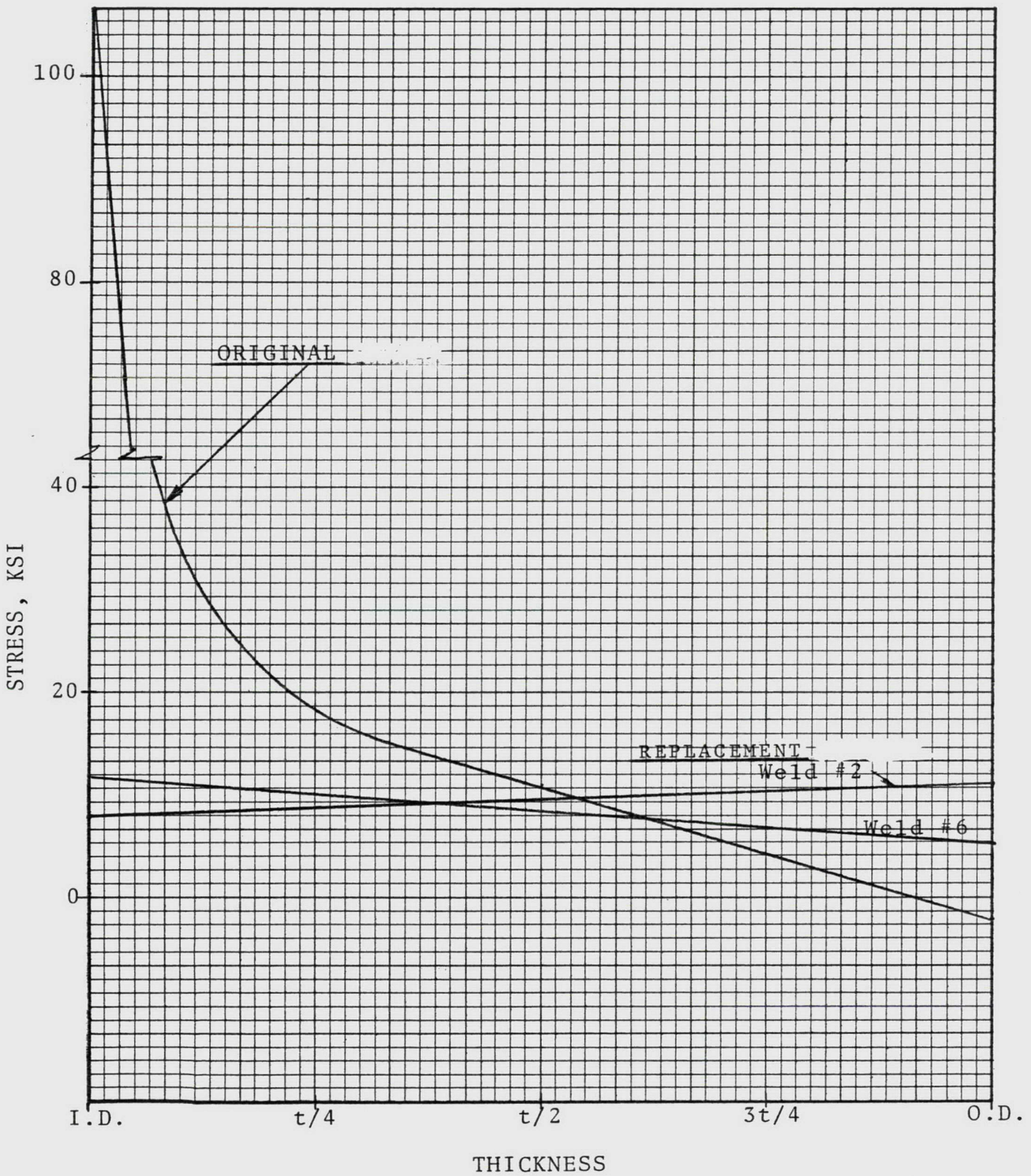

FIGURE V.B-3: Through Thickness Residual Stress Estimate for Butt Welded Pipe and for Nozzle Safe End (References V.B-1 and V.B-2)

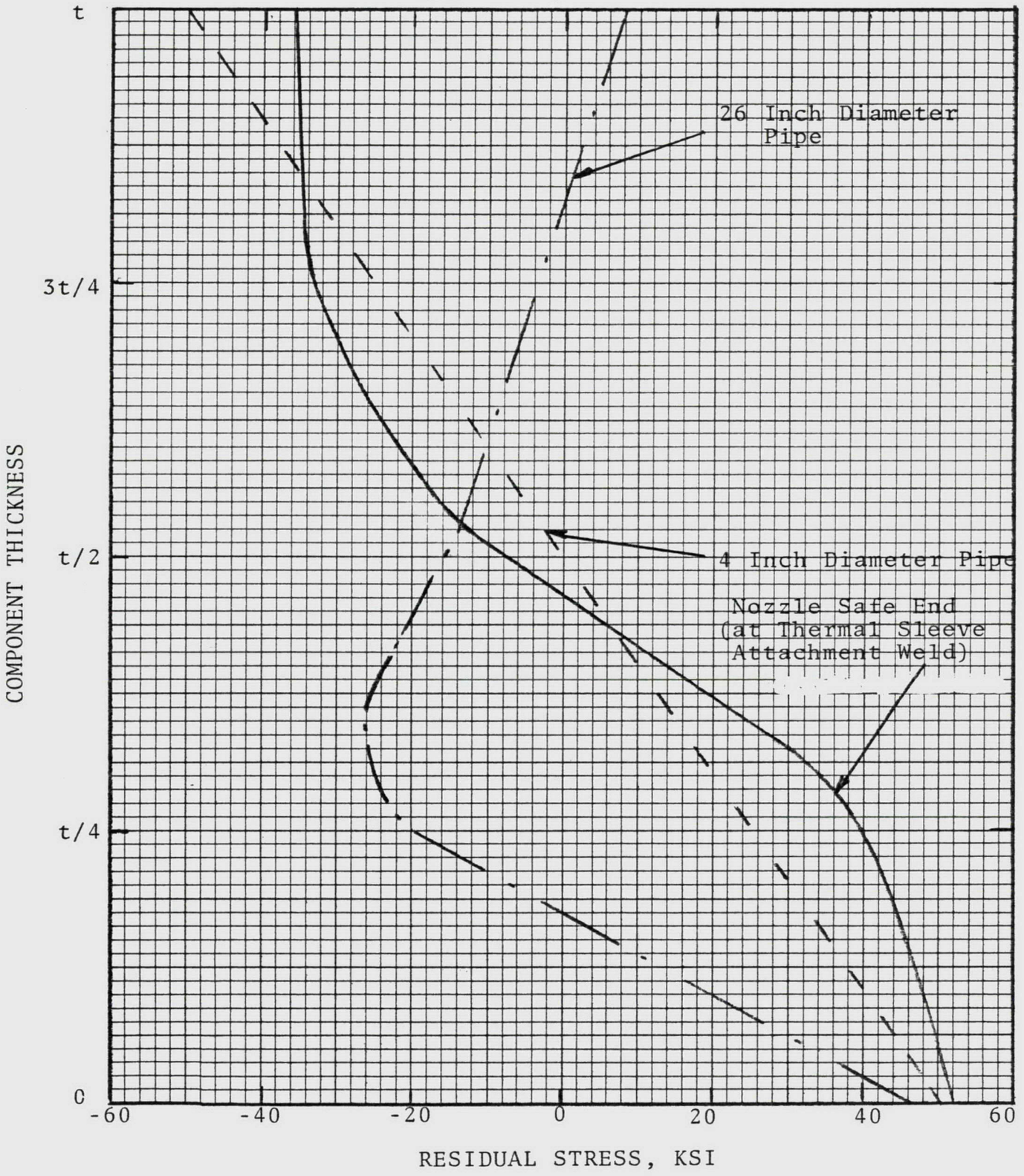

FIGURE V.B-4: Stress Intensity Factor as a Function of Crack Depth for Original and Replacement DAEC Safe Ends.

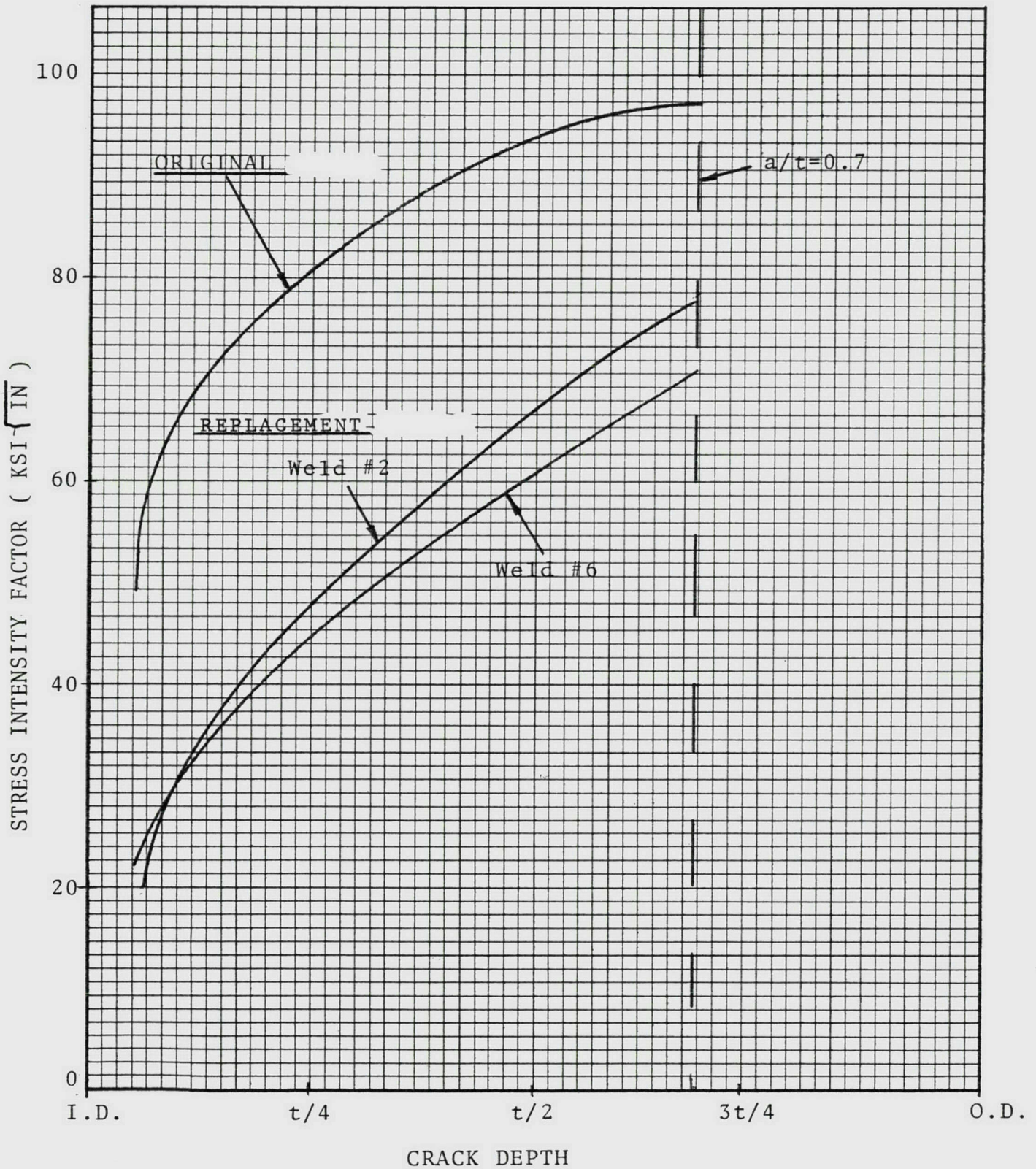

FIGURE V.B-5: DAEC Recirculation Nozzle Safe End
Crack Growth Estimates

Low Slope Crack Growth Law: $\frac{da}{dt} = 3.66 \times 10^{-7} (K)^{0.835}$

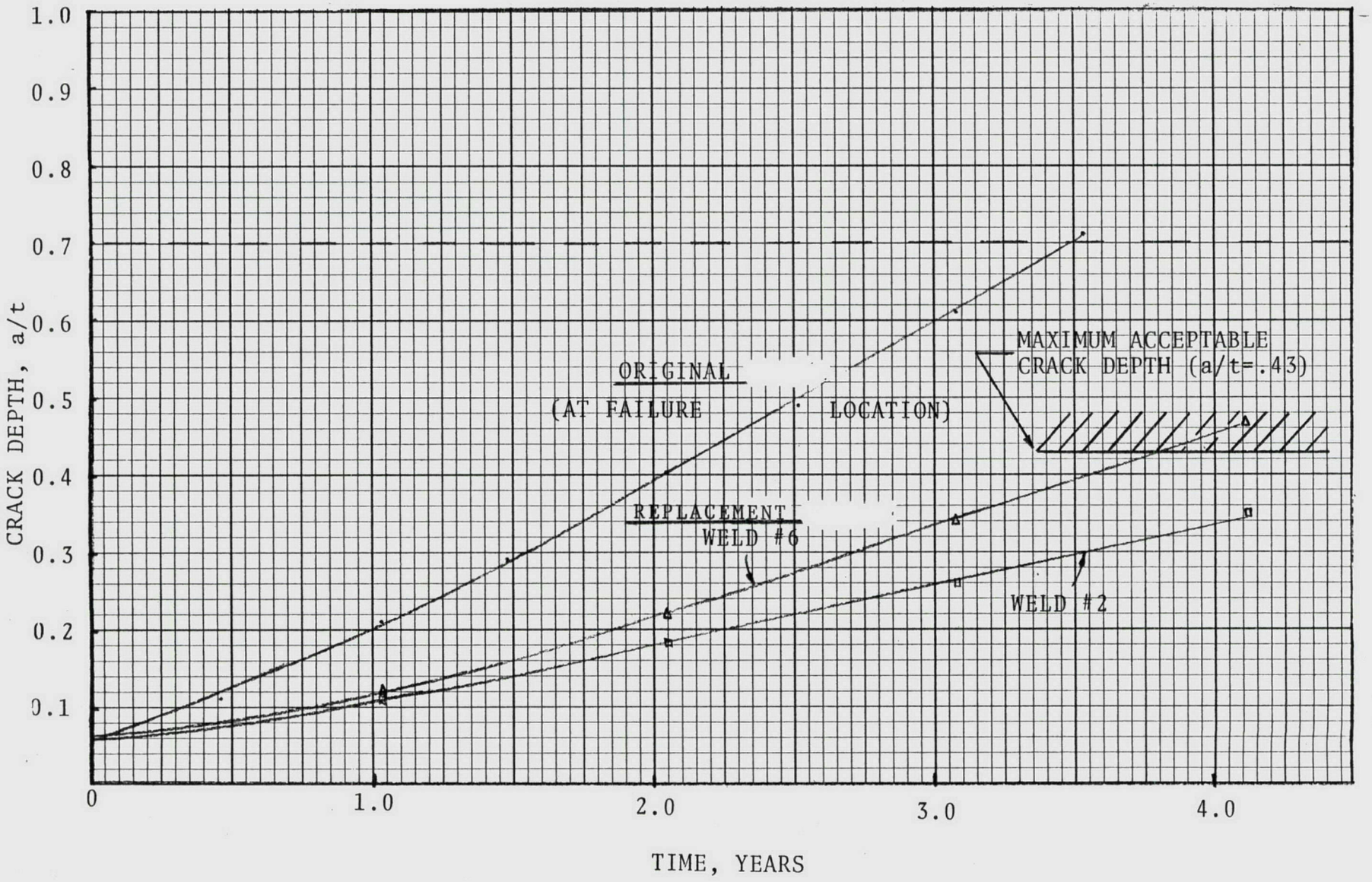

FIGURE V.B-6: DAEC Recirculation Nozzle Safe End
Crack Growth Estimates

High Slope Crack Growth Law: $\frac{da}{dt} = 5.17 \times 10^{-9} (K)^{1.935}$

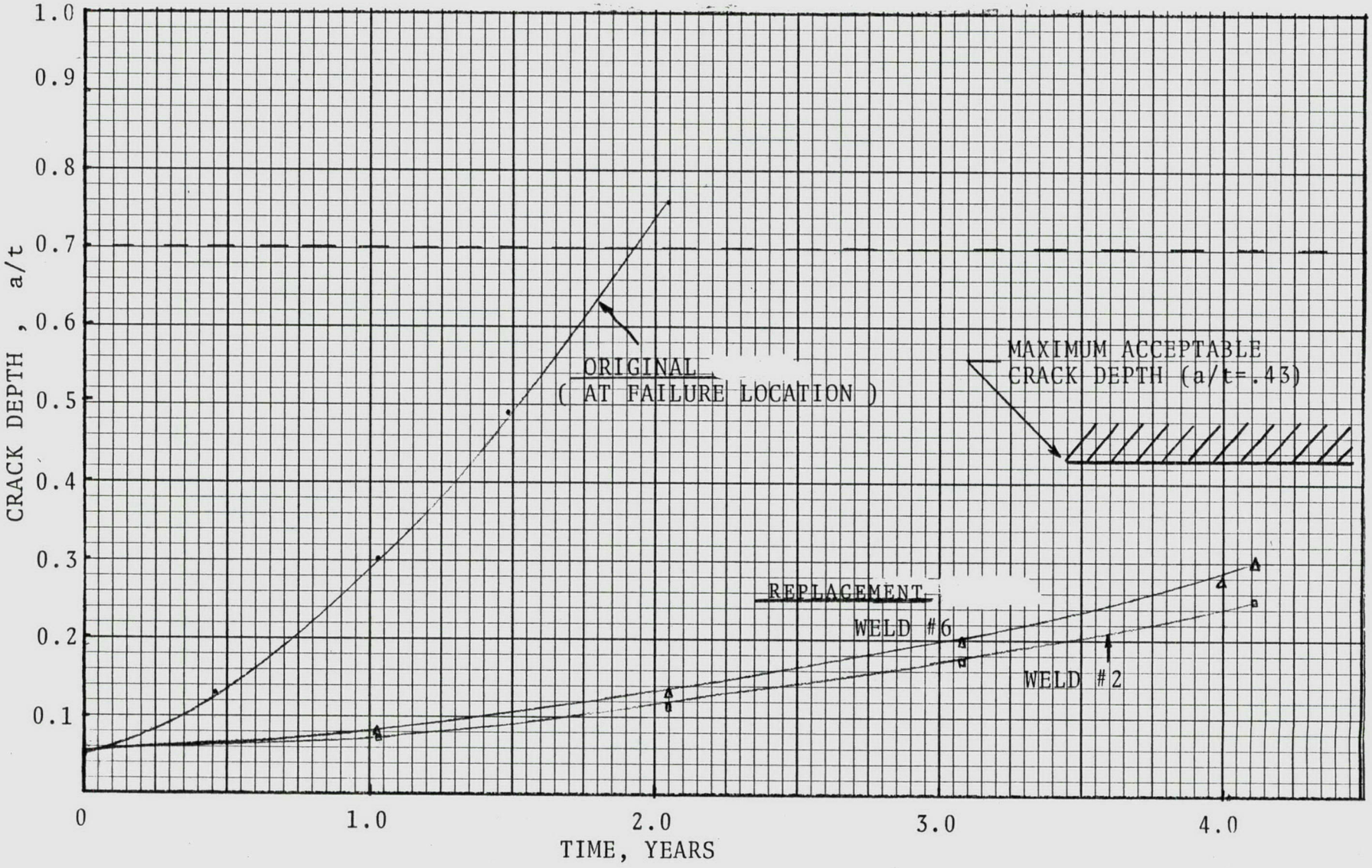

V.C MAXIMUM ACCEPTABLE CRACK DEPTH

In order to use the crack growth curves of Figures V.B-5 and V.B-6 to establish an ISI interval, an assessment must be made of the maximum acceptable crack depth. The basis of the acceptance criteria of the ASME Boiler and Pressure Vessel Code, Section XI for analytical evaluation of flaws detected during inservice inspection is that flaws are acceptable if they do not result in any reduction in design margin below that inherent in the original construction code stress limits. Paragraph IWB-3600 of Section XI provides specific limits for ferritic steel components which ensure, based on fracture mechanics considerations, that design margins are maintained.

For highly ductile materials such as Alloy 600 and stainless steel, however, the Section XI fracture mechanics approach does not provide a reasonable assessment of ultimate load carrying capacity of a component containing cracks. In fact, it has been shown experimentally (Refs. V.C-1 and 2) that a more elementary strength of materials approach, in which cracks are viewed as simply reducing the load bearing area of the component, provides a much more accurate assessment of load carrying capacity for circumferential cracks in austenitic steel piping. This strength of materials approach is thus applied to determine the maximum acceptable crack depth for postulated, 360^{o} cracks in the replacement safe-end welds #2 and #6.

The primary membrane and bending stress in Table II.C.1 is the governing primary stress intensity for weld #6. Based on the minimum design cross-sectional area at this location, a primary membrane and bending stess intensity equal to approximately 57 percent of the ASME Code allowable was determined in the stress report. Since this stress intensity results from an algebraic summation of the axial and radial stress components, and since the axial stress component varies linearly with cross sectional area, it is conservatively assumed that a 43 percent reduction in cross-sectional area at this location would result in a primary membrane plus bending stress exactly equal to the ASME Code limit. Thus, a postulated 360° crack would have to propagate to a depth greater than 43 percent of the design wall thickness before any reduction in load carrying capacity below the standard ASME Section III design margins would be experienced. Review of Table II.C.2 reveals that the primary stresses in Weld #2 are even lower than those in Weld #6, and thus 43 percent is used as a conservative approximation of the acceptable crack depth for weld #2 also.

The above assessment of design margins and acceptable crack depth implicitly assumes no loss of design margin due to increases in secondary and peak stresses. Such an assumption is justified by the basic self-relieving nature of secondary and peak stresses, which renders them incapable of leading to gross structural failure in a ductile material, and thus not a factor in assessing loss of design margin.

JLR:cas/61L2

The 43 percent acceptable crack depth determined above is shown as horizontal slashed lines on Figures V.B.5 and V.B.6 for the purpose of establishing a conservative interval for inservice inspection of the subject welds. Note that in most cases, the predicted crack growth curve does not even intersect the acceptable crack depth during the time interval considered in the analysis. The weld #6 curve based on the low slope crack growth law of Equation 1 does intersect the acceptable crack depth, however at approximately 3.8 years. Thus the analysis presented herein supports a minimum inservice inspection interval of 3.8 years based on a highly conservative set of assumptions. The following is a summary of some of the major conservatisms which have gone into establishing this inspection interval:

1. Cracking was always assumed to occur uniformly for 360° around the circumference of the piping, while all of the observed indications in the subject weld are relatively short in length, and any cracking postulated to occur as a result of the indications would be expected to be localized in nature.

2. Additional pipe thickness at the weld locations due to reinforcement at the weld outside diameter was ignored. All calculations were performed using the minimum design wall thickness.

JLR:cas/61L3

3. The crack growth curve used in establishing the 3.8 year inspection intervals was conservatively based on the low crack growth law in Figure V.B-6. Using the high slope crack grwoth law, which gives a more reasonable prediction of crack growth in the original safe end, would yield a longer inspection interval on the order of 5 years by extrapolation on Figure V.B-5.

4. No credit is taken for the time required to nucleate an active stress corrosion crack. With the low stress levels which exist in the replacement safe-end welds, crack initiation, if it occurs at all, would be expected to take much longer than in the original safe-end design.

REFERENCES

1. Kanninen, M. F., Broek, D., et al, "Mechanical Fracture Predictions for Sensitized Stainless Steel Piping With Circumferential Cracks," Battelle Columbus Laboratories, Final Report to Electric Power Research Institute, EPRI NP-192.

2. Watanabe, M., Mukai, Y., et al, "Mechanical Behavior on Bursting of Longitudinally and Circumferentially Notched AISI 304 Stainless Steel Pipes By Hydraulic and Explosion Tests," Osaka University, Japan.

V.D LEAK BEFORE BREAK

Although the design basis for nuclear plants includes a postulated pipe break (LOCA), piping and safe end systems are analyzed, materials are selected, and leak detection systems designed to assure that if a pipe or safe end should crack, that crack would grow to a leak and the leak would be detected before a crack reaches critical size. This concept has been called leak before break.

In general terms, the leak before break (LBB) concept is built on the fact that reactor piping and safe ends are fabricated from ductile materials which can tolerate large through-wall cracks without fracture under service type loads. This has been shown by fracture mechanics theory, supported by laboratory tests, full scale tests, and field experience. Further, it has been shown that through-wall cracks which leak at the rate of 5 gpm or less have significant margin before pipe rupture.

The bases for leak before break for axial flaws has been presented in GESSAR (Ref. III.D-1). These bases were subsequently expanded in the case of circumferential flaws and documented in NEDO-21000 (Ref. III.D-2). In the following sections, the technical bases for circumferential flaw evaluation has been updated to reflect recent test data and analytical development for predicting critical flaw dimensions. Although the following analyses were originally developed for stainless steel piping, because of similar mechanical properties and geometrics the same conclusions can be drawn for Alloy 600 safe end applications.

JLR:cas/61B14

Circumferential Crack Assessment

Recent work by General Electric has led to better modeling of circumferential critical crack phenomena than is reported in NEDO-21000 (Reference III.D-2). This modeling uses the Net Section Collapse Criterion (Reference III.D-3).

For materials exhibiting highly ductile behavior, such as BWR piping or safe ends, failure criteria based on brittle fracture or linear elastic fracture mechanics considerations are not valid since failure is characterized by gross yielding and subsequent plastic instability. In the following analysis it is assumed that a pipe with a circumferential crack is at the point of incipient failure when the net section at the crack forms a plastic hinge and the pipe is ready to collapse. The net section collapse criterion is simple to apply and has been shown to be effective in predicting failure of cracked ductile components by Electric Power Research Institute Report NP-192 (Reference III.D-4) and the NRC (Reference III.D-5).

In order to determine the point at which collapse occurs, for a circumferential crack of length, 1, and depth, d, located on the inside section of the pipe (Figure III.A.3-1), it is necessary to apply the equation of equilibrium assuming the the cracked section behaves like a hinge. For this condition the stress state at the cracked section is as shown in Figure III.D where the maximum stress is the flow stress of the material o_f. Further, the flow stress has been shown to be a function of the ultimate strength of material o_u and the yield strength o_y and can be

JLR:cas/61B15

approximated by $(o_u+o_y)/2$. The angle, B, at which stress inversion occurs can be determined for equilibrium in the longitudinal direction. If P_m is the primary membrane stress in the longitudinal direction in the uncracked section of the pipe, it can be shown that B is given by:

$$B = \frac{o_f\ (\pi - \frac{ad}{t}) \ - P_m\pi}{2o_f} \qquad \text{(Equation 1)}$$

The maximum primary bending stress, P_b, is determined by equating the moments in the crack section to the applied moments in the uncracked sections of the pipe when the flaw parameters are critical. In this case:

$$P_b = \frac{2o_f}{\pi} \qquad 2 \sin B - \frac{d}{t} \sin a \qquad \text{(Equation 2)}$$

Equations (1) and (2) together define the combinations of a and d/t for which failure by collapse will occur under the given applied stresses P_m and P_b.

For normal steady state conditions of operation, the only primary stress of significance is the PR/2t pressure stress. The bending stress due to dead weight is small and can be ignored.

By solving equations (1) and (2) for a through-wall crack with d/t = 1.0 it is demonstrated that a through-wall crack of up to 55% of the circumference can be tolerated with o_f = 50 Ksi and P_m = 5.4 Ksi. In other words, the critical crack length is 55% of the pipe circumference. For schedule 80 4" and 12" pipes we therefore obtain the following:

JLR:cas/61B16

Nominal Pipe Size (Schd 80), in.	Avg Wall Thick, In.	Circumferential Critical Crack Length, in.
4	0.337	6.9
12	0.687	20.7

The results are comparable to the axial critical crack length calculations. Either axial or circumferential critical crack lengths can therefore be compared to limiting crack length for 5 gpm leakage flow to assess safety margins for the leak detection system.

JLR:cas/61B17

Leakage Flow Rate for Circumferential Cracks

The maximum flow rate for blowdown of saturated water at 1000 psi is 55 lb/sec-in^2. Friction in the flow passages reduces this rate but can be ignored in piping geometries for leakages. The required crack size for 5 gpm saturated water flow, under these conditions, is

$$A = 0.0126 \text{ in.}^2$$

Given this area, and determining the crack opening displacement, w, the crack length 1 for a 5 gpm leakage rate can be determined.

For circumferential cracks, the crack opening displacement has been treated in NEDO-21000 and is similar to GESSAR except that the applied nominal stress is now equal to PR/2t, giving a longer crack length to yield a 5 gpm leak rate. In NEDO-21000, the comparison for the same 4" and 12" pipe sizes gives:

Nominal Pipe Size (Sch 80), In.	Avg Wall Thick, In.	5 gpm Crack Lengths, In.	Ratio (5 gpm)/(critical)
4	0.337	5.9	0.86
12	0.687	7.4	0.35

This comparison shows that even for the lower operating stress on the circumferential crack opening, substantial margin exists from the 5 gpm leakage crack length to the critical crack length.

JLR:cas/61B18

It is important to recognize that the failure of ductile piping with a long through-wall crack is characterized by large crack opening displacements which precede unstable rupture. Judging from observed crack behavior in the GE and BMI experimental programs involving both circumferential and axial cracks, it is estimated that leak rates at hundreds of gpm will precede crack instability. Measured crack opening displacements for the BMI experiments were in the range of 0.1 to 0.2 in. at the time of incipient rupture, corresponding to leaks of the order of 1 sq. in. in size.

The application of circumferential crack growth to the conditions found or postulated to exist on welds 2 and 6 is conservative. The conditions in question exist locally rather than circumferentially as discussed in Section II.D.

JLR:cas/61B19

REFERENCES

SECTION V.D

1. GESSAR, General Electric Standard Safety Analysis Report, 238 Nuclear Island, Docket STN 50-447, Section 5.2.7.

2. H. H. Klepfer, et. al., "Investigation of Cause of Cracking in Austenitic Stainless Steel Piping," NEDO-21000, July 1975.

3. S. Ranganath, "Failure Analysis Diagram for Circumferential Cracks in Austenitic Piping", May 26, 1978. GE letter RSFA-78-01.

4. "Mechanical Fracture Predictions for Sensitized Stainless Steel Piping with Circumferential Cracks", EPRI Report NP-192, Final Report September 1976.

5. "Review and Assessment of Research Relevant to Design Aspects of Nuclear Power Plant Piping Systems," NUREG-0307, Nuclear Regulatory Commission, July 1977.

JLR:cas/61B20

VI. INSERVICE INSPECTION

A baseline ultrasonic volumetric inspection of the recirculation system inlet nozzle replacement safe end pressure boundary welds has been conducted to the requirements of Section XI of the ASME Code. This inspection was however performed utilizing a 5% notch calibration technique providing greater sensitivity than the Code applied 10% notch calibration.

Section II.D described the acceptance of the above welds for ultrasonic inspection and the baseline inspection demonstrated that capability.

The crack growth analysis results presented in Section III indicate that growth of an assumed crack would not exceed Code limiting conditions within 3.8 years. We will, therefore, initiate an inservice inspection program for the above welds that will allow for inspection of all the welds within an inspection interval of two refueling outages. Fifty (50) percent of the welds will be ultrasonically inspected each refueling outage.

The above inspections will continue for 4 refueling periods and if no inspection results dictate a revision to the inspection requirements, then the inspection interval will be as described in the Repair Report dated 12/8/78.

JLR:cas/61J5

VII. LEAK DETECTION

A. Installed Leakage Detection Systems

The primary leakage detection system for the containment is the Drywell Floor Drain Sump system which is shown schematically in Figure VII-1. Other leak detection systems are indicated on Figure VII-2.

The Drywell Floor Drain system is capable of detecting a one gpm leakage increase above a one gpm leak baseline through use of the sump fill timer. Actual leakage rate trend is through use of the sump discharge integrator. A four-hour interval is required to obtain an accurate leak rate measurement. This four-hour leak rate is determined and plotted in the control room.

In addition to the above quantitative system, the following parameters are used to qualitatively indicate leakage increases:

(1) drywell temperature

(2) drywell radiation (iodine, particulate, gaseous), and

(3) containment atmospheric weight.

JLR:cas/61J1

A plot of the above parameters monitored June 14-17, 1978 is included as Figure VII-3.

B. Plant Operability Criteria

Since February 1975 the DAEC has implemented the criteria as requested in IE Bulletin No. 74-10B, which is as follows:

1. If the reactor coolant leakage detection system for unidentified drywell leakage indicates, within a period of 4 hours or less, either an increase in unidentified leakage to twice the determined normal rate of unidentified leakage or an increase in the rate of unidentified leakage by two (2) gpm or more:

   a) Initiate plant shutdown immediately, and

   b) Determine the source of increased unidentified leakage prior to resuming operation. The rate of unidentified leakage, if from sources other than those of concern in IE Bulletins 74-10A, 74-10B, and 75-01, will be added to the identified leakage rate for the drywell prior to resuming operation.

      (In no case shall the rate of leakage exceed that specified in the technical specifications without those actions required by the technical specifications being taken.)

JLR:cas/61J2

2. An attempt to verify the suspected increase of unidentified leakage in the drywell will be performed by observing the data from other equipment used in detecting unidentified leakage. This equipment includes drywell airborne particulate radioactivity monitors, drywell airborne gaseous radioactivity monitors, and drywell relative humidity monitors.

JLR:cas/61J3

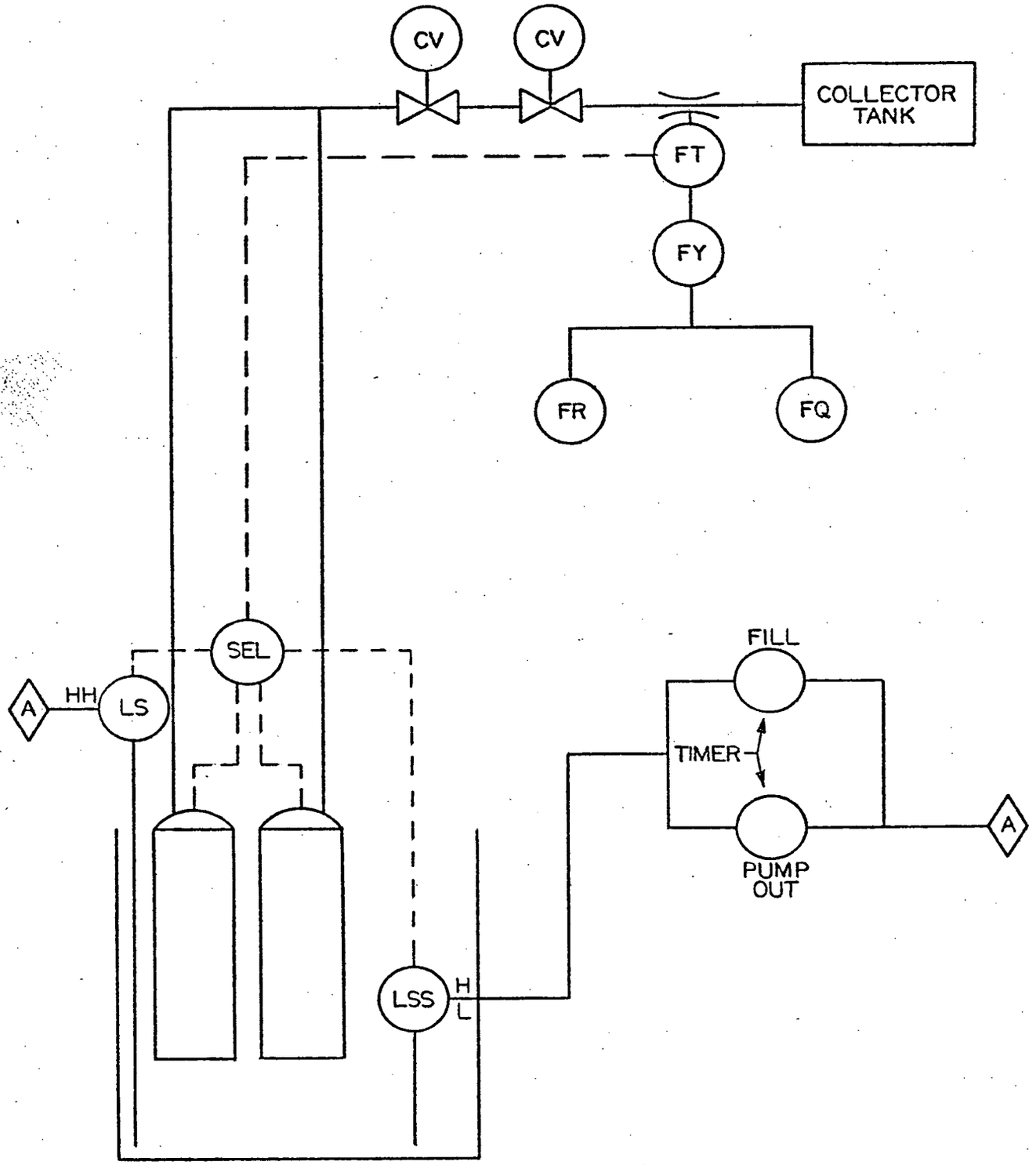

KAM
11/14/78

FIG. VII-1

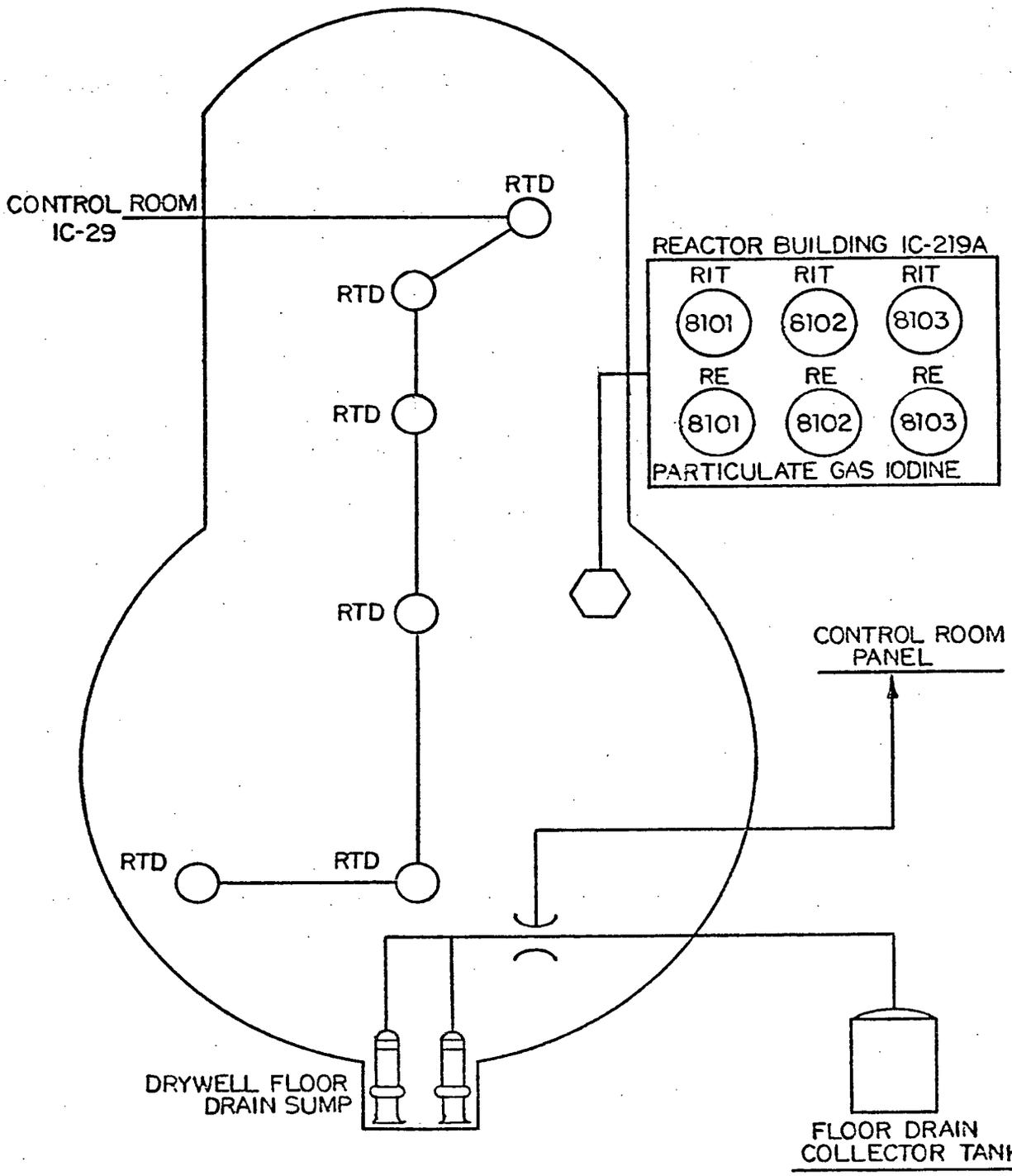

LEAK DETECTION

FIG. VII-2

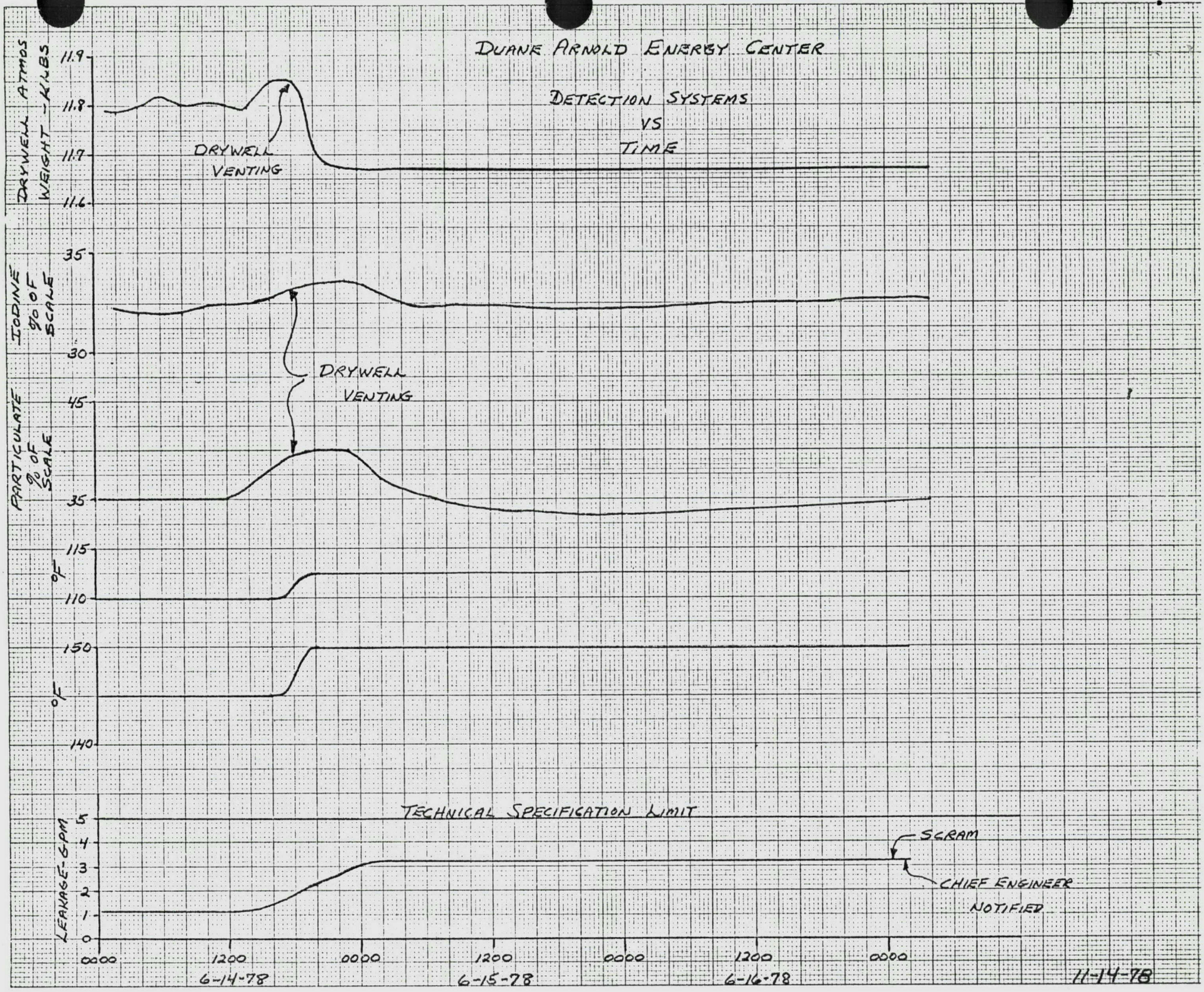

Figure VII-3